PARAMETERS ESTIMATION BASED ON RECURSIVE EXTENDED LEAST-SQUARES METHOD IN DC DISTRIBUTION SYSTEMS AND INTERIOR PERMANENT MAGNET SYNCHRONOUS MOTORS

by

Jiayue Xu

B.Eng, The University of Liverpool, 2016

A THESIS SUBMITTED IN PARTIAL FULFILLMENT OF

THE REQUIREMENTS FOR THE DEGREE OF

MASTER OF APPLIED SCIENCE

in

THE FACULTY OF GRADUATE AND POSTDOCTORAL STUDIES

(ELECTRICAL AND COMPUTER ENGINEERING)

THE UNIVERSITY OF BRITISH COLUMBIA

(Vancouver)

February 2019

The following individuals certify that they have read, and recommend to the Faculty of Graduate and Postdoctoral Studies for acceptance, a thesis/dissertation entitled:

Parameters Estimation Based on Recursive Extended Least-Squares Method in DC Distribution Systems and Interior Permanent Magnet Synchronous Motors

submitted by Jiayue Xu in partial fulfillment of the requirements for

the degree of Master of Applied Science

in Electrical and Computer Engineering

Examining Committee:

Dr. Juri Jatskevich, Electrical and Computer Engineering
Supervisor

Dr. William Dunford, Electrical and Computer Engineering
Supervisory Committee Member

Dr. Ryozo Nagamune, Mechanical Engineering
Supervisory Committee Member

Abstract

Adaptive control is widely used in modern control systems to maintain optimal system performance when the plant parameters are unknown and/or varying with time. Various system identification methods have been developed to estimate the system parameters in real time, which allows a parameter-related adaptive controller to be accordingly calibrated under parameter variation conditions. In this thesis, two practical applications of online parameters estimation are introduced: one the online source impedance identification for self-stabilizing controller design in dc distribution systems; and the adaptive controller design in interior permanent magnet synchronous motor (IPMSM) drive systems.

In dc distribution systems, the parameters of source impedances are crucial for load controller design to guarantee the stability of source-load interface. Since the source impedance may vary when the system configuration changes, the online impedance estimation is necessary for designing advanced self-stabilizing controllers with “plug-n-play” functionality. In this thesis, an innovative technique is proposed for parametric estimation of source impedance using the recursive extended least-squares (RELS) method in conjunction with impulse and pseudo-random binary sequence (PRBS) injections. Rigorous simulation studies demonstrate that the proposed technique yields direct results while providing advantages over traditional ac sweep and commonly used discrete Fourier transform (DFT) techniques. To further verify the feasibility of the proposed method in the real-time environment, the proposed online parameters estimator is implemented and validated on the Typhoon and Opal-RT hardware-in-the-loop (HIL) platform.

Moreover, the proposed methodology is extended to parameter-estimation-based adaptive control to mitigate the impact of parameter variations on the maximum torque per ampere (MTPA) operation of IPMSM drive systems. Specifically, a parameter estimator that exploits the RELS algorithm is established to accurately estimate the main parameters of the machine in real time, which enables calibration of the optimal current vector angle that is critical in the MTPA operation of IPMSMs. Extensive simulation studies have been carried out to verify the effectiveness and robustness of the proposed strategy.

Lay Summary

Online system parameter identification plays a key role in modern adaptive controller design for systems whose parameters are unknown and/or varying with time. In this thesis, an innovative technique is proposed for parametric estimation using the recursive extended least-squares (RELS). Two practical applications of online parameters estimation are introduced: source impedance identification in dc distribution systems; and the parameter-estimation-based adaptive controller in interior permanent magnet synchronous motors (IPMSMs). Rigorous simulation studies and hardware-in-the-loop (HIL) experiments verify the feasibility and effectiveness of the proposed method in real-time applications, and demonstrate that the proposed technique yields advantages over prior state-of-the-art estimation techniques.

Preface

Many of the research results presented in this thesis have been published in conference proceedings and/or will be submitted for peer review. In all publications, I am the primary contributor for deriving equations, developing models, running simulations and implementing hardware verifications under the supervision of Dr. Juri Jatskevich. My supervisor Dr. Juri Jatskevich also helped me writing and revising each paper. The conference papers resulting from this thesis and additional contributions by the co-authors are listed below.

Chapter 3 is based on the following conference paper:

J. Xu, Y. Huang, N. Amiri, J. Jatskevich, and O. Pizniur, "Online source impedance identification in dc distribution systems using the recursive extended least-squares method," in *Proc. IEEE 18th Work. Con. Mod. Power Electron.*, Padova, Italy, Jun. 2018, pp. 1-7.

The detailed model and average model of the dc distribution system in Section 3.1 are provided by Oleksandr Pizniur. Hua Chang and Dr. Yaqoob Muhammad provided help in hardware implementation and conducting the experiments described in Section 3.3.1.3. Dr. Juri Jatskevich, Dr. Yingwei Huang and Navid Amiri provided useful discussions, revisions, and proofread of the manuscript.

Chapter 3 and **Chapter 4** are based on the following journal paper:

J. Xu, Y. Huang, J. Xia, J. Jatskevich, "Online source impedance and parameters estimation in dc distribution systems using the recursive extended least-squares method," to be submitted.

Dr. Juri Jatskevich and Dr. Yingwei Huang provided useful discussions, revisions, and proofread of the manuscript. Jinhui Xia provided help in the digital signal processor coding for hardware implementation.

Chapter 5 and **Chapter 6** are based on the following conference paper:

J. Xia, J. Xu, Y. Huang, J. Jatskevich, Y. Guo and X. Zhang, "Parameter-estimation-based adaptive MTPA control for interior permanent magnet synchronous motors", in *Proc. IEEE 2019 6th Int. Con. Control Deci. Info. Tech. (CoDIT)*, Paris, France, 2019.

The MTPA control strategy and first draft of this paper was initiated by Jinhui Xia. I provided all simulation model and results related to the parameter estimation which have been proposed in this thesis. Dr. Juri Jatskevich, Dr. Yingwei Huang, Dr. Yuanbo Guo and Dr. Xiaohua Zhang provided useful discussions, revisions, and proofread of the manuscript.

Table of Contents

List of Tables

List of Figures

List of Symbols

In this thesis, scalars are written using italic fonts [e.g., n_a], and vector and matrices are denoted by bold letters [e.g., $\mathbf{y}$]. In addition, hatted letters are used to denote estimated variables [e.g., $\hat{\boldsymbol{\theta}}$].

Only basic variables are aggregated in this section; all other variables are defined explicitly throughout the thesis.

$A(z^{-1})$, $B(z^{-1})$, $C(z^{-1})$	Polynomials of output signal, input signal and noise signal
C_d	Passive damping capacitance in the damping circuit
f	Polynomial
$\mathbf{G}$	Transfer function of the plant in the form of a group of complex numbers
i^o, v^o	Steady-state values of current and voltage
$i_{q,d}$	Stator currents in *qd* reference frame
I_s	Stator current
$\mathbf{K}$	Gain value matrix
$L_{q,d}$	Inductances in *qd* reference frame
L_{tl}	Parasitic inductance in the transmission cable
$\mathbf{P}$	Covariance matrix
R	Stator resistance
$\mathbf{R}$	Random walk matrix
r_0	Random walk constant
R_d	Passive damping resistance in the damping circuit

R_o	Output impedance of flyback dc/dc converter
R_{tl}	Parasitic resistance in the transmission cable
T_s	Sampling time
$\mathbf{y}$, $\mathbf{u}$	Input signals, output signals
n_a, n_b, n_c	Order number of Polynomials $A(z^{-1})$, $B(z^{-1})$, $C(z^{-1})$
$u(k)$, $y(k)$, $e(k)$, $\varepsilon(k)$	Input signal, output signal, noise signal, and prediction noise signal in discrete domain
$v_{q,d}$	Stator voltages in *qd* reference frame
$x_i^{(k)}$, i=1,…,d, k=1,…n.	The ith root value in the kth iteration for polynomial f
Z	Impedance
$\mathbf{Z}_{DFT}$	Impedance results obtained from discrete Fourier transform in the form of a group of complex numbers
Z_{in}	Input impedance of the load system
Z_{out}	Output impedance of the source system
$\hat{\boldsymbol{\theta}}$	Estimated parameter vector
$\boldsymbol{\varphi}$	Regression vector
λ	Forgetting factor
λ_f	Flux linkage
γ	Current angle
γ_M	Optimal current angle
τ	Time constant
ω_e	Machine electrical angular velocity

$\Delta i(k)$, $\Delta v(k)$	Small signal values of current and voltage

List of Abbreviations

ac	Alternating Current
APA	Affine Projection Algorithm
AML, RML_2	Approximate Maximum-Likelihood
ARMAX	Moving Average with eXogenous Inputs
AVM	Average-Value Model
dc	Direct Current
DER	Distributed Energy Resources
DFT	Discrete Fourier Transform
DIBS	Discrete-Interval Binary Sequence
DM	Detailed Model
DSP	Digital Signal Processor
HIL	Hardware-in-the-Loop
IFOC	Indirect Field-Oriented Control
I/O	Input/Output
IPMSM	Interior Permanent Magnet Synchronous Motor
LUT	Look-Up Table
MLBS	Maximum-Length Binary Sequence
MTPA	Maximum Torque Per Ampere
PI	Proportional-Intergral
PRBS	Pseudo-Random Binary Sequence
RELS, RML_1	Recursive Extended Least-Squares
RLS	Recursive Least-Squares

RPWM	Random Pulse-Width Modulation
SCADA	Supervisory Control and Data Acquisition
SISO	Single Input and Single Output
TCP/IP	Transmission Control Protocol/Internet Protocol

Acknowledgements

I would like to express my enduring gratitude to the faculty, staff and my fellow graduate students at UBC, who have inspired me to continue my work in this field. I owe particular thanks to my supervisor Dr. Juri Jatskevich, who provided me with an excellent opportunity to enlarge my vision of research. It was a great pleasure to be supervised by such a knowledgeable and hardworking professor, whose professional expertise and penetrating questions and encouragement have taught me to question more deeply and be creative in providing the solutions and answers.

I am grateful to Dr. William Dunford and Dr. Ryozo Nagamune for dedicating their valuable time and effort to serve on my examining committee, and for all of their useful feedback that have helped to improve the quality of this thesis.

I would like to thank my colleagues Dr. Yingwei Huang and Jinhui Xia for their invaluable comments and discussions of my research. I would like to thank my colleagues Dr. Yaqoob Muhammad, Jinhui Xia, Shaobo Yin, Dr. Zhenyu Shan, Hua Chang and Xinyu Zhang for their great help in setting up the experiments and programming the digital signal processor hardware. In addition, I would also like to thank all the colleagues from the UBC's Electric Power and Energy Systems research group including Oleksandr Pizniur, Navid Amiri, Xing Liang, Shuan Dong, Ahmed Sherwali, Javier Tarazona, Zejun Yang, Zhi Qu, Shuai Xu, Xiaotong Wang, Matin Rahmatian, Hanqing Lin, Mohammad Mahdavyfakhr, Hadi Aghazadeh and many others with whom I collaborated on research and spent countless hours in the lab.

Lastly, special thanks are owed to my parents and other family members, whose have supported me throughout many years of my education, both morally and financially.

Dedication

To my wonderful parents and friends

Chapter 1: Introduction

1.1 Motivation

System identification in an important area for many applications, and in this thesis it will be applied to two problems. Identification of source impedance in dc distribution systems is important for stabilizing the system especially when many electronic loads are non-linear and behave as constant power loads. In motor drive applications, the machine parameters can also vary significantly during the course of operation leading to detuning of controllers from original optimal operation strategies. These applications are considered for motivation of the proposed research.

1.1.1 Instability Issues in DC Distribution Systems

Due to increasing number of electronic loads that are inherently dc, lower energy losses, higher power quality, reduction in the number of energy conversion stages, and other advanced features, the dc systems are now becoming a realistic alternative for power distribution over the traditional ac systems, especially in vehicles [1], electric ships [2], and aircrafts [3], etc., and are now being considered for future buildings [4]. Figure 1. 1 illustrates an example generic dc distribution system which comprises an ac grid and a variety of distributed energy resources (DERs) power sources including renewable energy, battery bank and backup generator, etc.; several loads and appliances; energy storages for peak-shaving; a backup generator for supporting interruptions.

Such power-electronic-based systems consist of multiple converters creating interfaces at different voltage levels [5], whose stability can be assessed using the impedance-based criteria. Briefly, this criterion introduces the concept that the stability of the system-load interconnection depends on the ratio of the source impedance to the load impedance, which requires the detailed

impedance information both for source and load side [6]. However, obtaining the impedance of these source/load subsystems is generally challenging. The traditional approach requires injecting a series of small sinusoidal currents at known frequencies over a frequency range, where the impedances of the source and the load subsystems at the corresponding frequency can be calculated using the injected current and resulting voltage through frequency response analyzer [7]. The disadvantage of this technique is that the whole procedure of measurement takes a long time. Moreover, this offline method is not sufficient to guarantee the interconnection stability due to the variation of the impedance of both source side and load side. Alternative approaches include developing and analyzing models of the considered system with all its details and sub-systems. However, the traditional detailed model with switches cannot be easily linearized for small-signal impedance-based analysis, and instead equivalent dynamic average value models may be derived and used. However, deriving accurate average-value models for all components of the system and their interconnections requires a large amount of work that has to be done offline together with the actual hardware. Consequently, there is a significant need to investigate a reliable and efficient online impedance estimation method, which can be used for adaptive controllers to stabilize the interconnection in the dc distribution systems.

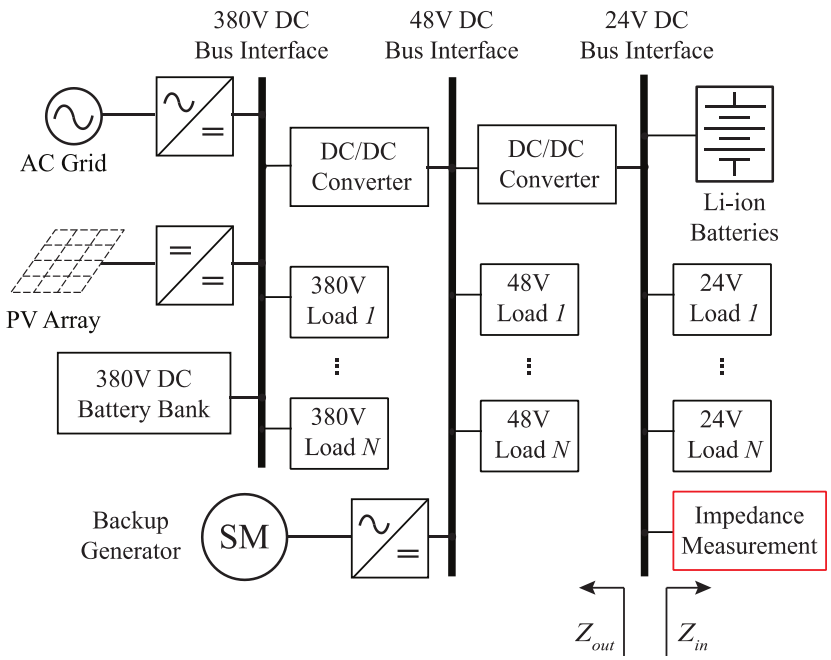

Figure 1. 1 Example generic dc distribution system with multiple sources and loads at several buses.

1.1.2 Compromised Efficiency Optimization of IPMSMs

Interior permanent magnet synchronous motors (IPMSMs) have many advantageous features including high efficiency, high torque density, and good reliability [8], [9], and such machines have broad range of applications in industry including emerging electric vehicles, high-speed railway, and wind turbines. A common technique to improve the efficiency of the IPMSM drive systems is called the maximum torque per ampere (MTPA) control, which calculates an optimal current vector between the *q*-axis and the *d*- axis currents to minimize the stator current under a given load torque [10]. However, the calculation of optimal current vector in MTPA control is dependent on the actual parameters of the motor. Therefore, the resulting efficiency may be decreased by the variations in several key parameters of the IPMSM. Consequently, it is desirable to develop a parameter-estimation-based adaptive MTPA controller that can detect the parameters online and update the controller to guarantee its optimal operation.

1.2 Literature Review

1.2.1 System Identification

System identification can be generally classified into non-parametric approach [11] and parametric approach [12]. The non-parametric approach uses the discrete Fourier transform (DFT) to capture the frequency response of the system, and is recommended for systems with an unknown structure/model, because it does not require to establish a mathematical model for the tested system. However, the information obtained from DFT is given as a vector of complex numbers for a range of frequencies, which generally can be presented in the form of Bode plots. To make use of such data points (e.g., for designing the adaptive controller), one needs to convert these data points into a transfer function, which requires to further extract the specific parameters. Moreover, the DFT method can be sensitive to noise especially in the high frequency range, resulting in spurious data points in the Bode plots [11]. Alternatively, the parametric approaches of system identification are able to provide direct parameter estimation of the tested system, while featuring self-calibration in case of the system uncertainty/noises. The parametric approaches have been proven as feasible tools for adaptive controller design [12]. Therefore, the parametric approach is considered in this thesis.

In the parametric approach considered in this thesis, the system is first represented by a discrete-time domain mathematical model, and then a recursive estimating algorithm is applied to identify the parameters of the model. For discrete-time modeling for the system, the Auto-Regressive with eXogenous inputs (ARX) model and Auto-Regressive Moving Average with eXogenous inputs (ARMAX) model are commonly used [13]. Both ARX and ARMAX models describe the general system as linear input/output model in terms of polynomials with one noise/disturbance input. However, the ARX model structure, due to its simplicity, is only able to

consider white noise. To improve the practicability, the ARMAX model considers a moving average of noise, which can present colored noise with more properties. This extended noise term endows the ARMAX model with invulnerability to the impact of bias in measurements and harmonics.

The recursive algorithms designed for ARX model is called the Recursive Least-Squares (RLS), and for ARMAX model can be the Recursive Extended Least-Squares (RELS or RML_1) and Approximate Maximum-Likelihood (AML or RML_2) [12]. Specifically, the RELS algorithm allows the estimated parameters of the system to be updated at each sample interval (using a sliding time window). The estimator based on the history information (in the parameters of transfer function) is used to obtain an estimate output, which is then compared with the measured output to generate a prediction error. This value in turn updates the parameters of the model. These recursive "predictor-corrector" calculations significantly save the computation time and make the online system identification possible.

Moreover, in practical applications the system parameters need to be properly tracked for variations before being applied to adaptive controller design. It is noted that, occasionally, the covariance matrix in the RELS algorithm may become very small when the system is working in steady-state operating mode. In this case, if one or more parameters suddenly change(s), the covariance matrix will be too small to allow the estimator to be updated with a faster speed. The traditional way to solve this issue is the forgetting factor technique [12], which is able to make the covariance matrix more sensitive to the system parameter variation. However, this technique requires a persistent excitation into the estimated system; otherwise, it will accelerate estimator wind-up. To resolve this issue, other techniques such as random walk algorithm, constant trace

algorithm, variable forgetting factors and adaptive forgetting factors have been applied to better track the parameters variations [12].

In summary, the state-of-the-art system identification methods applicable to the problems considered in this thesis are structurally depicted in Figure 2. 1. As shown in the figure, the ARMAX model and RELS algorithm are selected in this thesis due to their advantageous properties.

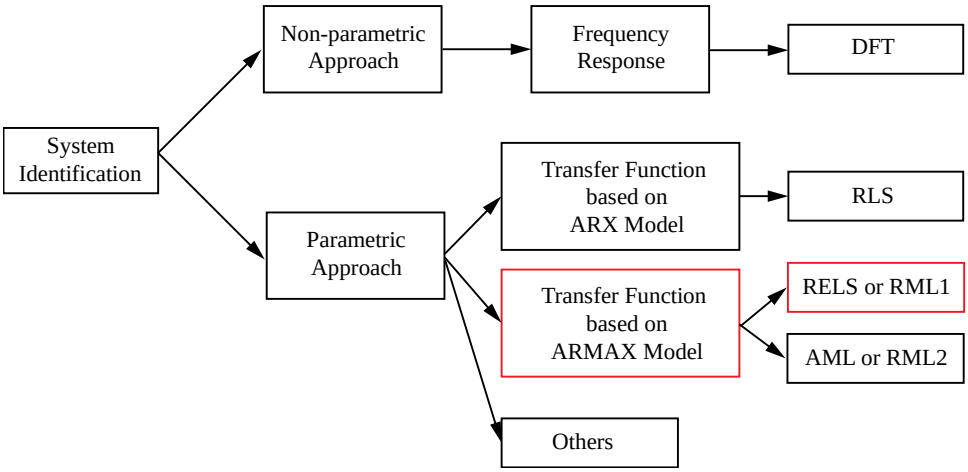

Figure 2. 1. Overview of system identification methods showing the approach considered in this thesis.

1.2.2 Injection-Based Impedance Estimation in DC Distribution Systems

As discussed in Section 1.1.1, online impedance estimation is a widely recognized system identification application, especially for source/load impedance measurement for adaptive controller design in dc distribution systems. To do so, the common approach (referred to as injection-based impedance estimation) firstly injects a disturbance signal into the system, and then analyzes the resulting small-signal transients and applies the system identification algorithm to calculate the impedance transfer function of the system.

Presently, the state-of-the-art work is mainly based on the DFT analysis (i.e., non-parametric approach) and focuses on improving the injection approaches [15]-[27]. According to the types of injection signal, the estimation approaches can be classified into large-signal injection methods [15]-[20] and small-signal injection methods [21]-[27]. The large-signal injection method injects into the bus interface a single impulse signal [15]-[19], or a piece-wise linear signal [20], which is easy to implement and requires a shorter processing period. The small-signal injection methods inject a broadband excitation, including random pulse-width modulation (RPWM) [21], pseudo-random binary sequence (PRBS) [22][23], maximum-length binary sequence (MLBS) [24], discrete-interval binary sequence (DIBS) [25], Ternary sequence [26], [27], etc. These small-signal injections are injected into the bus interface at a given operating point (without destabilizing the system), and have been applied to multiple input and multiple output (MIMO) systems [28]-[30]. After the injection, the entire response of resulting currents and voltages are needed to be stored and then analyzed using DFT to calculate the frequency response of the system impedance.

Because the DFT algorithm is difficult program in digital signal processor (DSP), most of the papers [15]-[30] studied the offline simulations to calculate the impedance, with exclusion of [15] that firstly implements the online impedance estimation in DSP and [19] in HIL simulations. In addition, since the DFT results are given in the form of a vector of complex numbers, the previous methods mainly rely on the bode plot of the identified impedance to access the stability of system/load interconnection, while only [17] applies curve fitting technique to further extract the resonant frequency and damping ratio for stabilizer design offline. In all the literature [15]-[30], the resulted frequency response of impedance can be highly affected by the system noise, especially in the high frequency range. More importantly, the obtained bode plots are not

parametric solutions, and from these bode plots one still needs to reconstruct the required impedance transfer functions.

In contrast, the impedance estimation based on parametric approach is more suitable for online adaptive controller design, since it can address the limitations of DFT as discussed in Section 1.2.1. So far, only one researcher applied this technique into online power grid impedance matrices calculation based on RLS [31], which however was studied with offline simulations.

1.2.3 Parameters Estimation of Interior Permanent Magnet Synchronous Motors

As discussed in Section 1.1.2, the machine parameters are required to be accurately detected in the real time to improve the performance of MTPA control. Several estimation methods have been applied to identify machine parameters offline or online. For offline approaches, the machine parameters are stored as functions of *q*- and *d*-axes currents in the look-up table (LUT) for optimum vector control [32] [33]. However, the LUT approach requires massive offline measurements and storage space in the controller.

For online approaches, several algorithms are applied into machine parameters estimation including spectrum-analysis-based approach [34], model-based approach [35] [36] and knowledge-based approach [37]-[43]. Spectrum-analysis-based approach injects sinusoid signals in the system, and computes the parameters by analyzing the corresponding harmonics via spectrum analysis [34]. However, to identify machine parameters in real time, this approach requires regularly signal injections at certain time intervals, which may affect the stability and efficiency of the IPMSM. Model-based approach is then proposed to overcome this drawback, which is able to calculate machine parameters through solving machine equations [35][36]. However, in this approach, the stator resistor of the motor is assumed to be a known constant and

the system is required to work in the steady state. Recently, knowledge-based approaches are attracting increased attention, including affine projection algorithm (APA) [37], [38], recursive least squares (RLS) algorithm [39]-[42] and artificial neural networks [43]. These algorithms have the capability of updating the estimated parameters recursively in real time based on the history information. Specially, the RLS algorithm has the advantages which is the capability of full machine parameters estimation, relatively low calculation requirement and small prior knowledge storage requirement.

1.3 Hardware-in-the-Loop Testing Platform

Hardware-in-the-loop (HIL) is a technique that is used in the developing or testing embedded systems. The HIL platform applied in this thesis is based on Opal RT-LAB Control Desk [44], which mainly includes the following tools:

- Simulation Model: MATLAB [46]/Simulink model [47]
- Supervisory Control and Data Acquisition Interface: LabVIEW[48]
- Real-time Simulator: OP5700

HIL based on RT-LAB is a powerful platform which is able to simulate the model, and receive or generate the desired signals of the model through I/Os in the real time, and provides the possibility for connecting digital signal processor (DSP) from the third-party with the simulation model in the real-time simulator. This system is mainly designed for model-based design and virtual prototyping, control prototyping, embedded control testing and data logging, and significantly improves the efficiency of testing embedded controllers, by reducing the risk, cost and overall time, and is therefore considered for in this thesis.

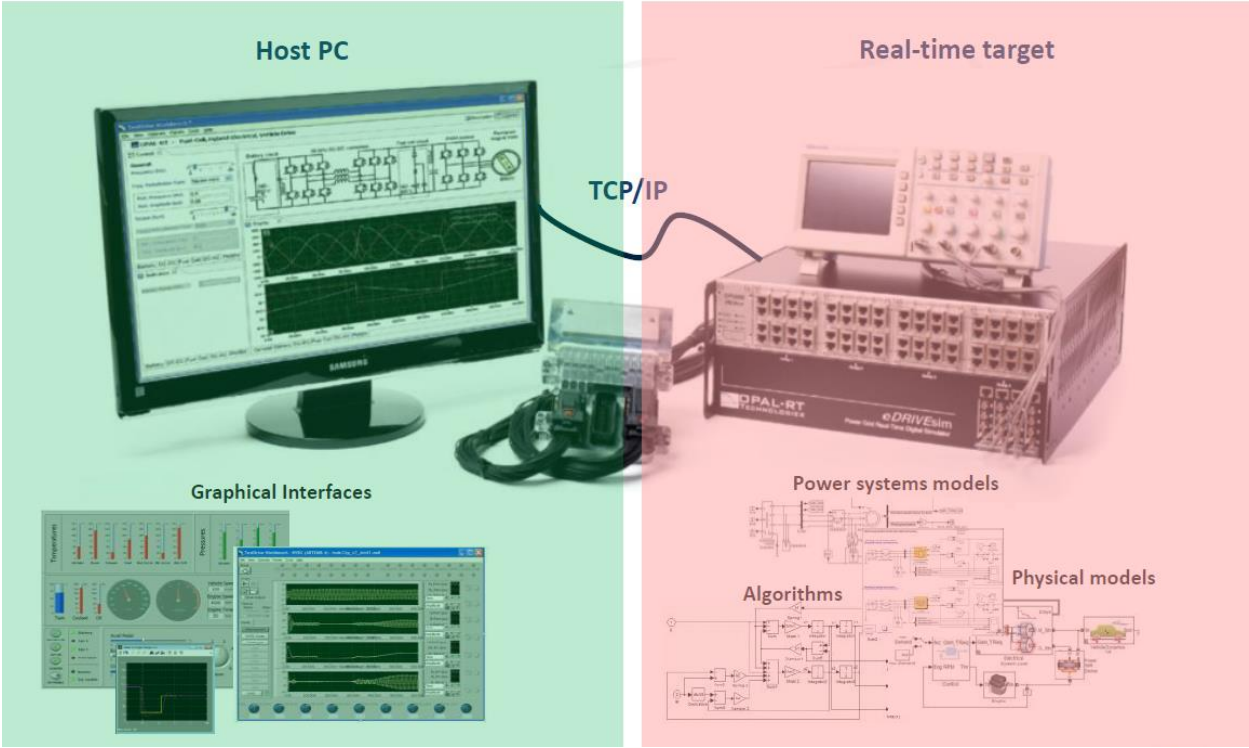

Figure 1. 2 Photo of real-time simulator OPAL-RT system [44].

1.4 Research Objectives

In this thesis, we aim to apply the RELS algorithm to parameter estimation of two practical industrial applications: 1) an online impedance estimator for the dc distribution system; and 2) online parameter estimator for IPMSMs. Both applications allow the estimated transfer function to be updated iteratively in real time, which yields a direct solution of transfer function with proper parameters and makes it possible to be implemented in adaptive controllers. The detailed objectives are summarized below:

Objective 1—Design an online source impedance estimator in dc distribution system based on RELS algorithm.

To guarantee the stability of source-load interface, the parameters of source impedances are crucial for load controller design. Since the source impedance may vary when the system configuration changes, it is necessary to design an online impedance estimator for source system, to properly extract the transfer function of the source impedance and parameters of filters in the source side. The traditional method (i.e., DFT method) and RELS method under impulse injection are compared to demonstrate the advantages of this proposed method. To mitigate the impact of the injection on the interconnection system stability, another type of injection (i.e. PRBS injection) is also introduced. The estimator performance including numerical properties, estimated error, and noise tolerance under impulse injection and PRBS injection are investigated.

Objective 2—Implement the proposed online impedance estimator in DSP and verify the technique based on HIL testing platform.

The proposed online impedance estimator should be verified in real time environment. To achieve this, we need to implement the proposed algorithm on HIL platform, which includes writing the code for impedance estimator in the DSP (i.e., TMS320F28335), developing the dc distribution system model in Simulink in the real-time simulator (i.e., OP5700) and designing the SCADA interface in LabVIEW. In this objective, the feasibility of the proposed estimator is investigated with different selections of system orders. The recommended configuration for impedance estimator in the real time environment are presented.

Objective 3—Design an online parameter estimation for adaptive MTPA controller for IPMSM.

For IPMSMs, the machine parameter variations caused by the demagnetization and temperature effects may influence the accuracy of MTPA operation. An online parameters estimator based on RELS algorithm is desirable for accurate adaptive MTPA control. The simulation platform of a speed servo control system of the IPMSM is to be established. Simulation case studies will be carried out to verify the effectiveness and robustness of the proposed RELS algorithm.

Chapter 2: System Identification and Parameters Estimation Methods

2.1 System Identification Methods

To set the stage for the development of practical applications, the methodology of both non-parametric approach and parametric approach of system identification are firstly introduced.

2.1.1 Non-Parametric Approach

Frequency response analysis has been proven as a straightforward and reliable method for system identification [11]. This is done by applying DFT method to measure the frequency spectrum of the desired system response following these steps:

1) Measure the input and output signals of the plant (denoted by **y** and **u**, respectively), and record with a finite length of data points (restricted as the number of 2^n).
2) Apply the DFT to the two obtained sequences of signals and calculate the transfer function of the plant **G** in the form of a vector of complex numbers, as

$$\mathbf{G}(e^{j\omega}) = \frac{\mathrm{DFT}(\mathbf{y})}{\mathrm{DFT}(\mathbf{u})}. \tag{2.1}$$

It is noted that the input power spectrum density is usually relatively low and unstable in the high frequency range, which results in significant noise data in the corresponding frequency. These noise data can be filtered by removing the corresponding unsuitable data in the input power spectrum density. In addition, the transfer function of measured system can be derived from the obtained frequency response through the curve fitting technique (i.e. RLS) offline.

2.1.2 Parametric Approach

2.1.2.1 Mathematical Model Structure

In the parametric approach, a discrete-time transfer function model of the system is developed with input signal $u(k)$ output signal $y(k)$, and noise signal $e(k)$. In this thesis, the model structure of Auto-Regressive Moving Average with eXogenous inputs (ARMAX) [13] is selected as

$$A(z^{-1})y(k) = B(z^{-1})u(k) + C(z^{-1})e(k)\,, \tag{2.2}$$

where $A(z^{-1})$, $B(z^{-1})$ and $C(z^{-1})$ are polynomials of proper orders (n_a, n_b, n_c respectively) as

$$\begin{cases} A(z^{-1}) = 1 + a_1 z^{-1} + \ldots + a_{n_a} z^{-n_a} \\ B(z^{-1}) = b_0 + b_1 z^{-1} + \ldots + b_{n_b} z^{-n_b} \\ C(z^{-1}) = 1 + c_1 z^{-1} + \ldots + c_{n_c} z^{-n_c} \end{cases}. \tag{2.3}$$

The signal flow of ARMAX is given in Figure 2. 2. It is worth mentioning that, the noise term $C(z^{-1})e(k)$ represents the white noise when n_c is 0. Otherwise, it represents the colored noise, which is useful when the harmonics or offsets exist in the measurement signals.

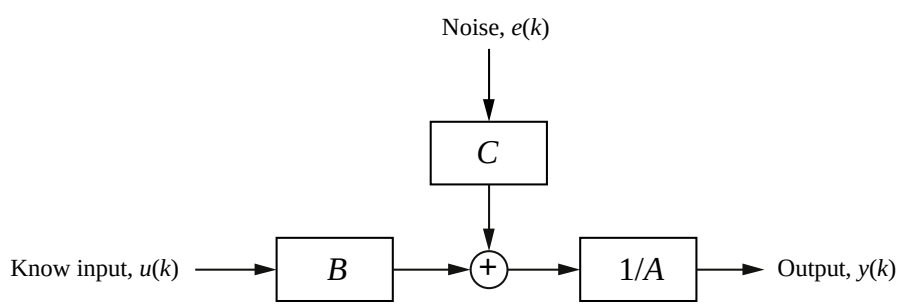

Figure 2. 2 Signal flow diagram of an ARMAX model.

2.1.2.2 Iteration Algorithm

For the recursive iteration algorithm, the RELS algorithm is selected in this thesis. The aim of this algorithm is to recursively estimate and update the parameters of the $A(z^{-1})$, $B(z^{-1})$ and $C(z^{-1})$ polynomials terms in (2.2), by measurement of input signal $u(k)$, output signal $y(k)$ and calculated noise signal $e(k)$. To do so, a parameter vector $\hat{\boldsymbol{\theta}}$ is constructed as

$$\hat{\boldsymbol{\theta}} = \begin{bmatrix} a_1 & \cdots & a_{n_a}, & b_0 & \cdots & b_{n_b}, & c_1 & \cdots & c_{n_c} \end{bmatrix}^T. \tag{2.4}$$

This parameter vector $\hat{\boldsymbol{\theta}}$ can be updated using the procedures summarized as follows:

1) Select the proper order of transfer function n_a, n_b, n_c, and initialize the estimated parameters $\hat{\boldsymbol{\theta}}(0)$ and covariance matrix $\mathbf{P}(0)$.

2) Construct the regression vector $\boldsymbol{\varphi}(k+1)$ consisting of history information as

$$\begin{aligned} \boldsymbol{\varphi}(k+1) = [&-y(k) \quad \cdots \quad -y(k-n_a+1), \\ &u(k+1) \quad \cdots \quad u(k-n_b+1), \\ &\varepsilon(k) \quad \cdots \quad \varepsilon(k-n_c+1)]^T, \end{aligned} \tag{2.5}$$

   where the noise term $e(k)$ in (2.2) is noticed to be replaced by the prediction error $\varepsilon(k)$, since noise normally cannot be measured.

3) Calculate the prediction error $\varepsilon(k+1)$ as

$$\varepsilon(k+1) = y(k+1) - \hat{y}(k+1) = y(k+1) - \boldsymbol{\varphi}^T(k+1)\hat{\boldsymbol{\theta}}(k), \tag{2.6}$$

   where $y(k+1)$ is the next measured output data, $\boldsymbol{\varphi}(k+1)$ is the next regression vector, and $\hat{\boldsymbol{\theta}}(k)$ is the previous estimated parameter vector.

4) Update the gain value $\mathbf{K}$, the covariance matrix $\mathbf{P}(k+1)$, and the predicted parameter vector $\hat{\boldsymbol{\theta}}(k+1)$

$$\mathbf{K} = \frac{\mathbf{P}(k)\boldsymbol{\varphi}(k+1)}{1+\boldsymbol{\varphi}^T(k+1)\mathbf{P}(k)\boldsymbol{\varphi}(k+1)}, \tag{2.7}$$

$$\mathbf{P}(k+1) = \mathbf{P}(k)\left[\mathbf{I} - \boldsymbol{\varphi}(k+1)\mathbf{K}^T\right], \tag{2.8}$$

$$\hat{\boldsymbol{\theta}}(k+1) = \hat{\boldsymbol{\theta}}(k) + \varepsilon(k+1)\mathbf{K}. \tag{2.9}$$

5) Wait until the next sampling time, return $\varepsilon(k+1)$ to Step 2) for the consecutive iteration and proceed to the next step.

2.2 Practical Applications of System Identification

Next, using the aforementioned non-parametric and parametric approaches of system identification, two practical applications including the dc distribution systems and IPMSMs will be investigated in this thesis. The procedure of system identification consists of three stages: 1) signal injection, 2) data analysis, and 3) parameters estimation. Specifically, the methods/algorithms utilized for each stage of the two applications are listed in Table 2. 1.

Table 2. 1 Two applications of system identification.

	DC Distribution Systems (Chapter 3 & 4)	**IPMSMs (Chapter 5)**
Signal Injection	Impulse, PRBS	Square Wave
Data Analysis	DFT, RELS	RELS
Parameters Estimation	Order reduction	N/A

2.2.1 Injection-Based Impedance Estimation in DC Distribution Systems

A simplified circuit for impedance measurement in dc distribution systems is shown in Figure 2. 3, where the source subsystem is represented as an ideal voltage source V_s with output impedance Z_{out}, and the load subsystem is represented as impedance Z_{load}. To obtain the dynamic response of system, it is common to inject a small disturbance current signal such as sinusoid

signals, impulse signals and PRBS signals into the interface as shown in Figure 2. 3. Following the current injection, the resulting small-signal deviations of voltage and current can be measured (in the discrete-time domain), and then applied with system identification methods to calculate the frequency response of the impedance using non-parametric (i.e., DFT) or parametric methods (i.e., RELS).

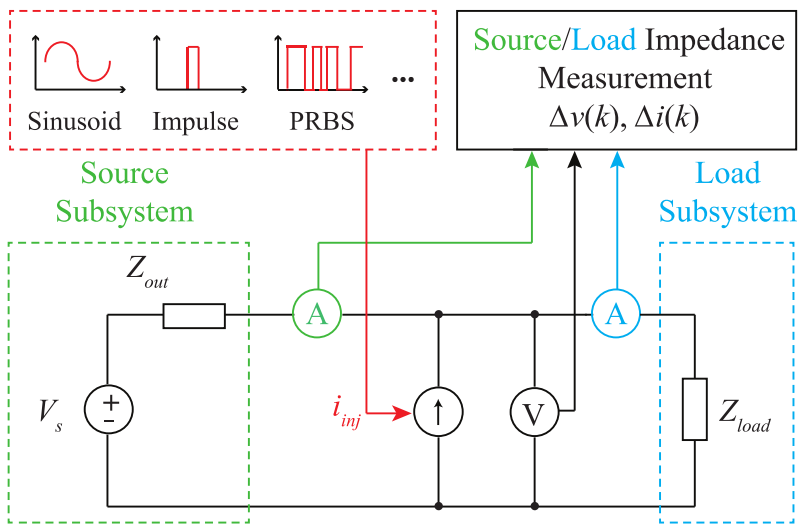

Figure 2. 3 Diagram for impedance estimation using injection-based methods.

2.2.1.1 DFT Algorithm for Online Impedance Estimation

The steps of implementation procedures of source impedance estimation based on DFT analysis are:

1) Given a system operating point with steady-state current i^o and voltage v^o, inject a small disturbance current i_{inj} into the bus interface;
2) Measure and record the transient response of current **i** and voltage **v** for the entire transient period;
3) Compute the small-signal deviations of current and voltage (Δ**i** and Δ**v**, respectively);

4) Apply (2.1) to obtain the frequency response of the impedance, i.e.,

$$\mathbf{Z}_{DFT}(e^{j\omega}) = \frac{\mathrm{DFT}(\mathbf{\Delta v})}{\mathrm{DFT}(\mathbf{\Delta i})}, \tag{2.10}$$

2.2.1.2 RELS Algorithm for Online Impedance Estimation

Alternatively, for impedance estimation based on parametric approach, we consider the RELS algorithm with ARMAX model as introduced in Section 2.1.2.1. Substituting small-signal of voltage $\Delta v(k)$ and current $\Delta i(k)$ into the ARMAX model (2.2), the relationship between $\Delta v(k)$ and $\Delta i(k)$ can be expressed as

$$\Delta v(k) = \frac{B(z^{-1})}{A(z^{-1})}\Delta i(k) + \frac{C(z^{-1})}{A(z^{-1})}e(k). \tag{2.11}$$

Since second term $C(z^{-1})e(k)/A(z^{-1})$ represents noise, it is usually neglected, which thereby yields

$$Z_{RELS}(z^{-1}) = \frac{\Delta v(k)}{\Delta i(k)} \approx \frac{B(z^{-1})}{A(z^{-1})}. \tag{2.12}$$

As seen in (2.12), the system impedance can be directly obtained in the form of a transfer function, which is a significant advantage over the non-parametric result (2.10). Moreover, compared with the DFT method, this method does not require to record the dynamic response of the system for the entire transient period.

Next, to estimate the parameters of $A(z^{-1})$, $B(z^{-1})$ and $C(z^{-1})$, the parameter vector $\hat{\boldsymbol{\theta}}$ is constructed as (2.4). This parameter vector $\hat{\boldsymbol{\theta}}$ can be updated applying the RELS algorithm as illustrated in Figure 2. 4. The procedure is summarized as follows:

1) Select the order of transfer function n_a, n_b, n_c, and initialize the estimated parameters $\hat{\boldsymbol{\theta}}(0)$ and covariance matrix $\mathbf{P}(0)$.

2) Given a system at steady-state operating point (i^o, v^o), inject a small disturbance current i_{inj} into the bus interface;

3) Compute the small-signal deviations of current $\Delta i(k)$ and voltage $\Delta v(k)$ based on the measured values $i(k)$ and $v(k)$;

4) Feed $\Delta i(k)$ and $\Delta v(k)$ as input $u(k)$ and output $y(k)$ signals into the RELS algorithm, as shown in Section 2.1.2.2;

5) Construct the resulted transfer function of impedance using (2.3) and (2.12).

6) Reduce the transfer function order if needed, calculate the parameters of the source system.

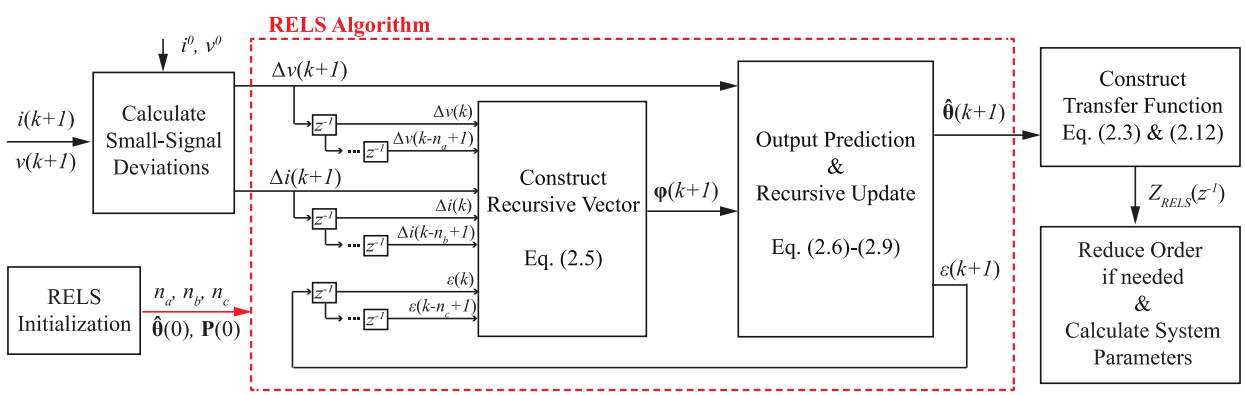

Figure 2. 4 Block diagram of applying the RELS algorithm for injection-based impedance calculation.

It is also noted that the accuracy of this impedance estimation depends on proper selection of the order of the ARMAX model. In practice, to improve the noise tolerance ability of RELS algorithm, it is necessary to increase the order of transfer function to guarantee that enough length of history current and voltage data for iterative calculations have been taken. This is specifically

designed for single input and single output (SISO) system, which is able to significantly eliminate the main drawback of noise sensitivity of RELS algorithm.

Despite preferable high order of ARMAX model to increase the noise tolerance ability of RELS algorithm, this may also cause some unnecessary poles and zeros in the obtained transfer function in the high frequency range. If the impedance transfer function is obtained with an unnecessary high order, the estimator needs to reevaluate/reduce the system order, before extracting the source parameters. This procedure consists of four stages: 1) estimation of dc gain, poles and zeros calculation, 2) poles and zeros selection, 3) reconstruction of impedance transfer function, 4) parameters extractions. Specifically, in stage 1) the poles and zeros calculation is implemented using Durand Kerner method as introduced in Section 2.2.1.3; and the execution of following stages will be further discussed in Section 3.2 after the model structure of the source impedance is defined.

2.2.1.3 Durand Kerner Root Finding Algorithm

Durand-Kerner method is a simple but effective method to find complex roots of a polynomial simultaneously [49]. Define a polynomial f of degree d and assumed it is monic, the roots $\mathbf{x}^{(0)}$ of f are initially set as,

$$\mathbf{x}^{(0)} = (x_1^{(0)}, x_2^{(0)}, \cdots, x_d^{(0)}). \tag{2.13}$$

Using Durand-Kerner method, the following formula is used to iterate until the desired iteration number n (which is user specified) is reached

$$x_i^{(k+1)} = x_i^{(k)} - \frac{f(x_i^{(k)})}{\prod_{\substack{j=1 \\ j\neq i}}^{d} (x_i^{(k)} - x_j^{(k)})}, \text{ for } i = 1, 2, \ldots, d, \text{ and } k = 0, 1, \ldots, n, \tag{2.14}$$

where k represents the index number for iteration. It is also noted that this algorithm requires operations in the order of $O(n \cdot d^2)$, which is time-consuming and may affect the total CPU time for system parameters calculation, which will be demonstrated in Chapter 4.

Chapter 3: Source Impedance Estimation of DC Distribution Systems

3.1 DC Distribution System Modeling

The considered dc source is a commercial converter (CXDF 48-24/2 kW prototype) installed in the dc distribution system of UBC Fred Kaiser Building. Figure 3. 1 depicts the circuit diagram of this source as a six-phase interleaved flyback converter, each having PWM signal inputs with phase shift [50]. Since it is impossible to linearize the detailed model, the corresponding average-value model (AVM) shown in Figure 3. 2 with double loop voltage control [51] is used to obtain the reference frequency response. The converter output also includes cables and an *RC* damping circuit as shown in Figure 3. 3. The detailed parameters of this system are listed in Appendix A.

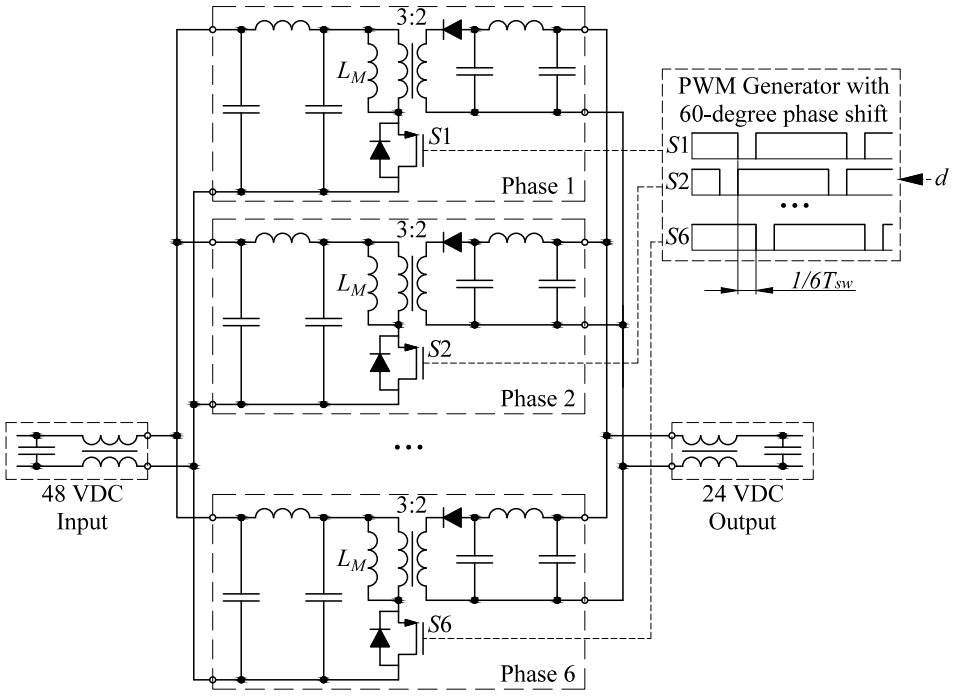

Figure 3. 1 Circuit diagram of the detailed model of the six-phase interleaved flyback dc-dc converter [51].

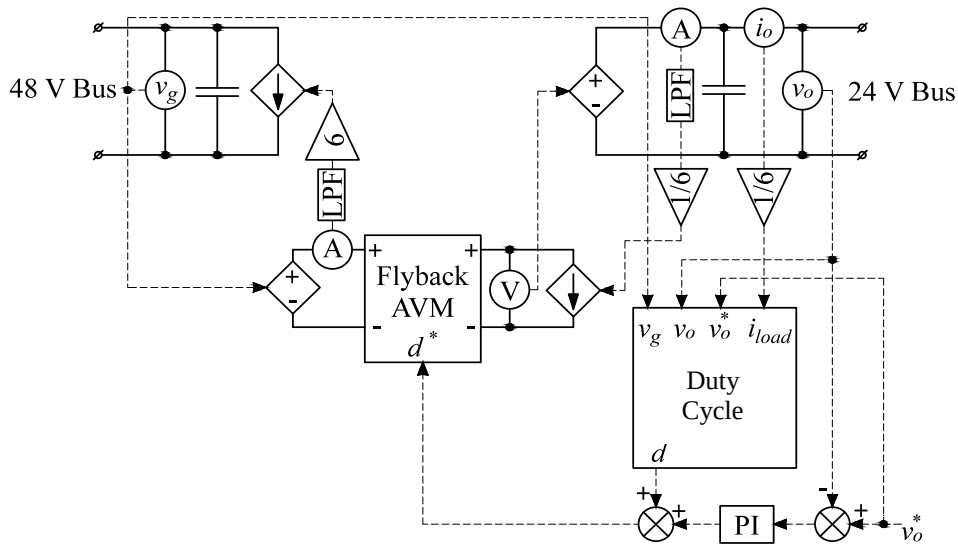

Figure 3. 2 Circuit diagram of the AVM of the six-phase interleaved flyback dc-dc converter [51].

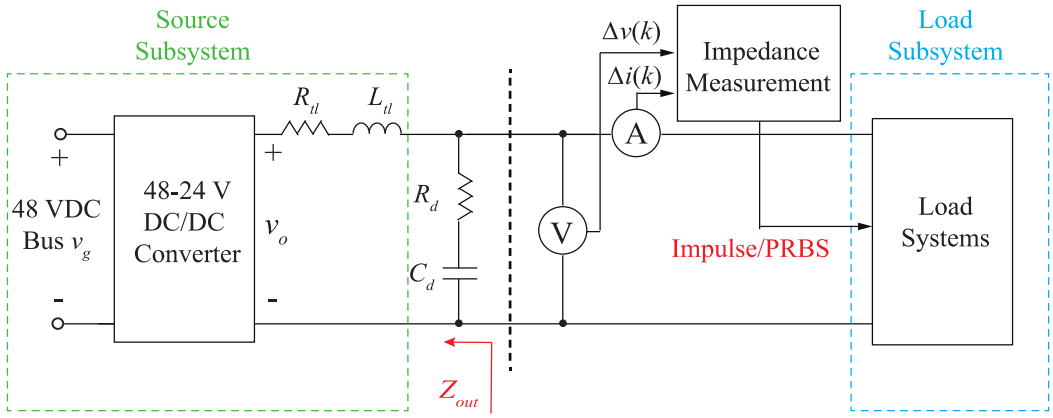

Figure 3. 3 Simplified circuit diagram of the considered source converter with connection cables and damping circuit.

To verify whether the simulation models are accurate, the impulse injection is applied here. To generate this kind of excitation, a load perturbation study of switching off/on a parallel resister R_{prtb} is carried from 0.1s to 0.104s. The parameters of the perturbation test are listed in Appendix B. The transient responses of the system under the perturbation test are shown in Figure 3. 4, where lines “Exp”, “Sim-DM”, and “Sim-AVM” denote the experiment results, the results predicted by

the detailed model and by the AVM, respectively. The test results verify consistency of all three subject models.

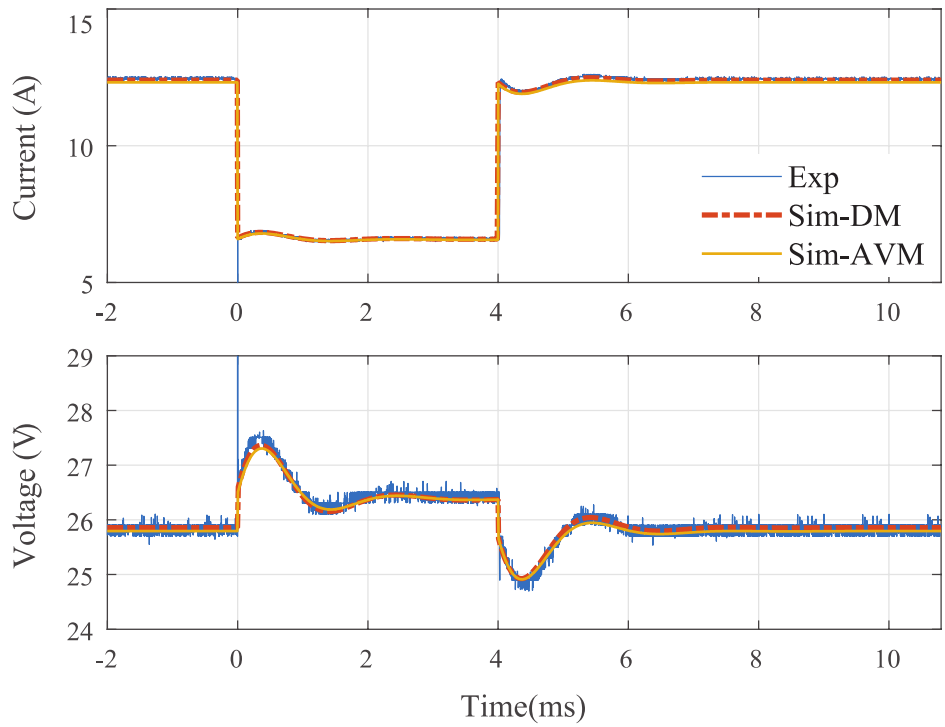

Figure 3. 4 Transient response of the system under the perturbation test.

3.2 Source Impedance Modeling and Estimation

As seen in Figure 3. 3, the total output impedance of the converter system consists of two parts: 1) the output impedance of the considered dc/dc converter in series with the transmission cable represented by its equivalent resistance and inductance (R_{tl} and L_{tl}), and 2) the damping circuit (R_d and L_d).

To analytically calculate the source impedance, it is noted that the output impedance of the considered CXDF 48-24/2kW prototype converter is generally small. By examining the dc gain of the converter, its output impedance can be simplified as resistance R_o, and then included into the output line resistance R_l as

$$R_l = R_o + R_{tl} \,. \tag{3.1}$$

Therefore, the total source output impedance $Z_{out}(s)$ may be expressed by the transfer function of the following form,

$$\begin{aligned} Z_{out}(s) &= (L_{tl}s + R_l) \,||\, (\frac{1}{C_d s} + R_d) \\ &= \frac{R_d s^2 + (\frac{1}{C_d} + \frac{R_d R_l}{L_{tl}})s + \frac{R_l}{L_{tl}C_d}}{s^2 + \frac{R_d + R_l}{L_{tl}} s + \frac{1}{L_{tl}C_d}} \,. \end{aligned} \tag{3.2}$$

The Bode plots of the output impedance of the AVM model and the reduced-order model (3.2) are shown in Figure 3. 5, which verifies the consistency of both models.

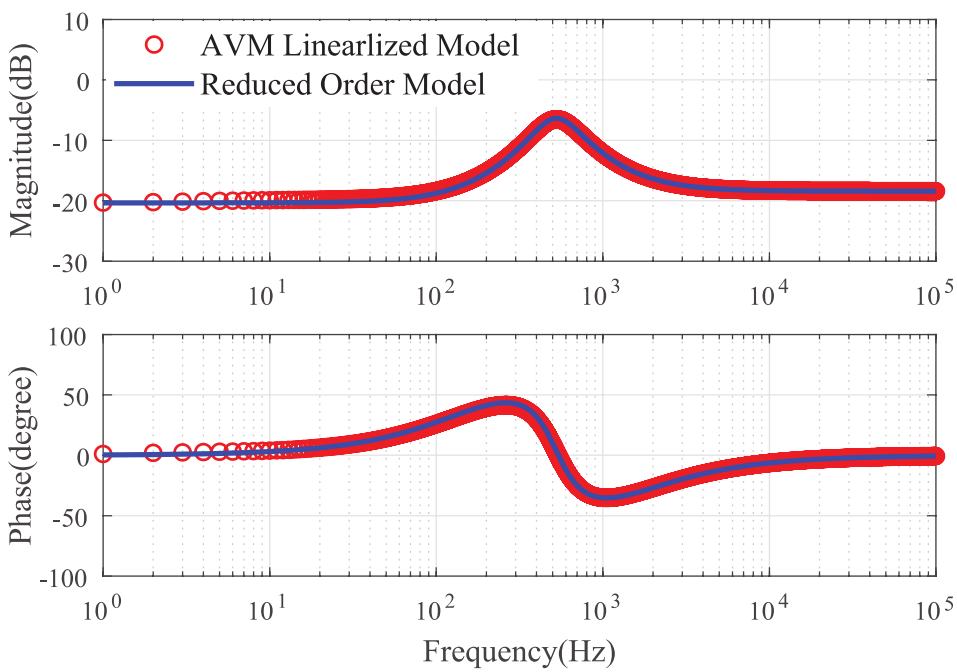

Figure 3. 5 Frequency domain response of the output impedance of the AVM model and the reduced-order model.

From (3.2), the transfer function of the source impedance can be constructed in zero-pole-gain format as

$$\begin{aligned} Z_{out}(s) &= k_s \frac{(s-z_{s\_1})(s-z_{s\_2})}{(s-p_{s\_1})(s-p_{s\_2})} \\ &= \frac{k_s s^2 - k_s(z_{s\_1}+z_{s\_2})s + k_s z_{s\_1} z_{s\_2}}{s^2-(p_{s\_1}+p_{s\_2})s + p_{s\_1}p_{s\_2}} \end{aligned}, \tag{3.3}$$

where k_s is the gain, $\mathbf{z}_{s\_1,2}$ are the zeros, and $\mathbf{p}_{s\_1,2}$ are the poles of (3.2). The dc gain of (3.3) can be expressed as

$$D = Z_{out}(s=0) = k_s \frac{z_{s\_1} z_{s\_2}}{p_{s\_1} p_{s\_2}}, \tag{3.4}$$

Comparing (3.3) with (3.2), one can obtain that

$$\begin{cases} R_l = D \\ R_d = k_s \\ L_{tl} = \dfrac{R_d + R_l}{p_{s\_1}+p_{s\_2}} \\ C_d = \dfrac{p_{s\_1}+p_{s\_2}}{p_{s\_1}p_{s\_2}(R_d+R_l)} \end{cases}. \tag{3.5}$$

Since the results of RELS algorithm is in the discrete-time domain, $Z_{out}(s)$ in (3.3) needs to be further discretized with sampling time T_s using the zero-order-hold as,

$$\begin{aligned} Z_{out}(z^{-1}) &= (1-z^{-1})\mathrm{Z}\left[\frac{Z_{out}}{s}\right] \\ &= (1-z^{-1})\mathrm{Z}\left[\frac{R_d s^2 + \left(\dfrac{1}{C_d}+\dfrac{R_d R_l}{L_{tl}}\right)s + \dfrac{R_l}{L_{tl}C_d}}{s\left(s^2+\dfrac{R_d R_l}{L_{tl}}s+\dfrac{1}{L_{tl}C_d}\right)}\right] \\ &= (1-z^{-1})\mathrm{Z}\left[\frac{R_l}{s} + \frac{p_1(s+\alpha)}{(s+\alpha)^2+\omega^2} + \frac{p_2\omega}{(s+\alpha)^2+\omega^2}\right] \end{aligned}, \tag{3.6}$$

where

$$\begin{cases} \alpha = \dfrac{R_d + R_l}{2L_{tl}} \\ \omega = \sqrt{\dfrac{1}{L_{tl}C_d} - \alpha^2} \\ p_1 = R_d - R_l \\ p_2 = \dfrac{-\dfrac{R_d^2 + R_l^2}{2L_{tl}} + \dfrac{1}{C_d}}{\omega} \end{cases}, \tag{3.7}$$

and T_s represents the sampling time. The transfer function can be further organized into the form of ARMAX format as,

$$Z_{out}(z^{-1}) = \frac{b_{0\_ref} + b_{1\_ref} z^{-1} + b_{2\_ref} z^{-2}}{1 + a_{1\_ref} z^{-1} + a_{2\_ref} z^{-2}}. \tag{3.8}$$

where

$$\begin{cases} b_{0\_ref} = p_1 + R_l = R_d \\ b_{1\_ref} = -p_1 - (p_1 + 2R_l)e^{-\alpha T_s}\cos\omega T_s + p_2 e^{-\alpha T_s}\sin\omega T_s \\ b_{2\_ref} = p_1 e^{-\alpha T_s}\cos\omega T_s - p_2 e^{-\alpha T_s}\sin\omega T_s + R_l e^{-2\alpha T_s} \\ a_{1\_ref} = -2e^{-\alpha T_s}\cos\omega T_s \\ a_{2\_ref} = e^{-2\alpha T_s} \end{cases}. \tag{3.9}$$

The transfer function (3.8) can be iteratively obtained applying the RELS algorithm as illustrated in Figure 2. 4. Ideally, the order of ARMAX model should be set as n_a=2, n_b=2, n_c=1 for ideal source impedance according to (3.8) and Figure 3.3.

However, because the RELS algorithm is noise sensitive, in practical applications it is necessary to increase the ARMAX model order to improve the noise tolerance ability. To do so, assuming the ARMAX model order is selected as N_{High}, the estimated transfer function of the identified impedance is,

$$Z_{RELS\_N_{High}}(z^{-1}) = \frac{b_0 + b_1 z^{-1} \cdots + b_{N_{High}} z^{-N_{High}}}{1 + a_1 z^{-1} + \cdots + a_{N_{High}} z^{-N_{High}}}. \tag{3.10}$$

For (3.10), its poles and zeros are denoted as p_{z_1}, …, p_{z_NHigh}, and z_{z_1}, …, z_{z_NHigh}, respectively, and the dc gain of (3.10) is

$$\hat{D} = Z_{out}(z^{-1} = 1) = (b_0 + \sum_{i \in I} b_i) / (1 + \sum_{i \in I} a_i), \mathbf{I} = \{1,\ 2,\ \ldots N_{High}\}. \tag{3.11}$$

Next, one needs to apply proper order reduction technique to eliminate the unnecessary poles and zeros in the high frequency range. This gives the reconstructed transfer function expressed by the selected poles (i.e., $\hat{p}_{z\_1}$, $\hat{p}_{z\_2}$) and zeros (i.e., $\hat{z}_{z\_1}$, $\hat{z}_{z\_2}$),

$$Z_{RELS\_2nd}(z^{-1}) = \hat{k}_z \frac{(z - \hat{z}_{z\_1})(z - \hat{z}_{z\_2})}{(z - \hat{p}_{z\_1})(z - \hat{p}_{z\_2})}, \tag{3.12}$$

where

$$\hat{k}_z = \hat{D} \frac{(1 - \hat{p}_{z\_1})(1 - \hat{p}_{z\_2})}{(1 - \hat{z}_{z\_1})(1 - \hat{z}_{z\_2})}. \tag{3.13}$$

The selected poles and zeros are then transferred into continuous-time domain according to

$$-s = \frac{1}{T_s} \ln \frac{1}{z}, \tag{3.14}$$

and the estimated dc gain $\hat{D}$, selected poles $\hat{p}_{s\_1}$, $\hat{p}_{s\_2}$ and zeros $\hat{z}_{s\_1}$, $\hat{z}_{s\_2}$ can be obtained in *s*-domain accordingly. Finally, parameters of the source impedance can be calculated using (3.5). The overall procedures of system order reduction and parameter extraction are summarized in Figure 3.6, which is fed from the RELS algorithm results shown in Figure 2. 4

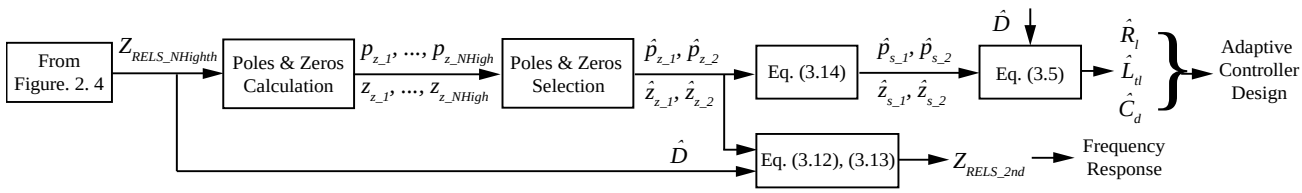

Figure 3. 6. Block diagram of order reduction and parameters extraction.

3.3 Computer Studies and Experimental Tests

To demonstrate the impedance estimation performance based on different types of recursive algorithms and injections, two scenarios are studied in this Chapter in various simulation case studies, as summarized in Table 3. 1. Therein, 1) Scenario 1 compares the impedance estimation based on impulse injection while using RELS algorithm and DFT algorithm; and 2) Scenario 2 compares the impedance estimation based on RELS algorithm while using impulse and PRBS injections. To give a thorough insight into the performance of estimator, the following aspects are investigated: 1) frequency response of impedance, 2) numerical comparison of algorithms, 3) system parameters estimation, 4) noise tolerance and performance of order selections.

Table 3. 1 Details of two scenarios in Chapter 3.

	Scenario 1		**Scenario 2**	
Load System	Passive Load	Passive Load	Active Load	Active Load
Case Study	Case 1	Case 2, 3	Case 4a, 4b	Case 5a, 5b
Signal Injections	Impulse	Impulse	Impulse, PRBS	Impulse, PRBS
System Identification	DFT, RELS	DFT, RELS	DFT, RELS	RELS
Inclusion of Noise	No	Yes	No	Yes

3.3.1 Scenario 1: Impedance estimation based on impulse injection while using RELS algorithm and DFT algorithm

In this scenario, a passive load (simplified as a constant resistor) is connected to the source system illustrated in Figure 3. 3, which is convenient to implement in the real experimental environment. Also, the impulse injection is applied, which is implemented through the perturbation test as demonstrated in Section 3.1. The purpose of studying this scenario is to compare the overall performance of impedance estimation using DFT and RELS algorithms.

To verity the advantages of RELS over DFT method, three case studies are performed: 1) Case 1: Ideal simulation without measurement noise; 2) Case 2: Simulation with measurement noise; and 3) Case 3: Experiment test.

3.3.1.1 Case 1: Simulation without System Noise

To demonstrate the accuracy of the proposed RELS algorithm, the load perturbation test is carried out as demonstrated in Section 3.1. Firstly, the ideal voltage and current responses [See Figure 3. 4, line Sim-DM] are used and fed to the impedance estimation, where the $\Delta\mathbf{i}$ and $\Delta\mathbf{v}$ are measured at a sampling frequency of 1 MHz. The initial settings for the proposed RELS algorithm are as follows: the ARMAX model order is set as n_a=2, n_b=2, n_c=1, the parameter vector $\boldsymbol{\theta}(0)$ is set as a zero vector, and the covariance $\mathbf{P}(0) = 10^6\mathbf{I}_6$.

Applying the RELS algorithm, the transfer function is directly calculated as a parametric solution:

$$Z_{RELS\_Case1}(z^{-1}) = \frac{0.1283 - 0.2454z^{-1} + 0.1172z^{-2}}{1 - 1.976z^{-1} + 0.9767z^{-2}}. \tag{3.15}$$

The Bode plots of the source output impedance obtained using the subject impedance estimation methods are shown in Figure 3. 7. Therein, the reference solution (obtained through offline linear analysis of the AVM model) and the results from the DFT method are also included. As seen in Figure 3. 7, the DFT method starts to attain the frequency response from 61.03 Hz, which is due to the limitation of the sampling frequency and capacity of samples of the DFT method and shows noise in the high frequency range. In contrast, the RELS method yields frequency response that is consistent with the reference solution in the entire range of 1-10^5 Hz, without noticeable error. This verifies the superior accuracy of the RELS method over the DFT methods.

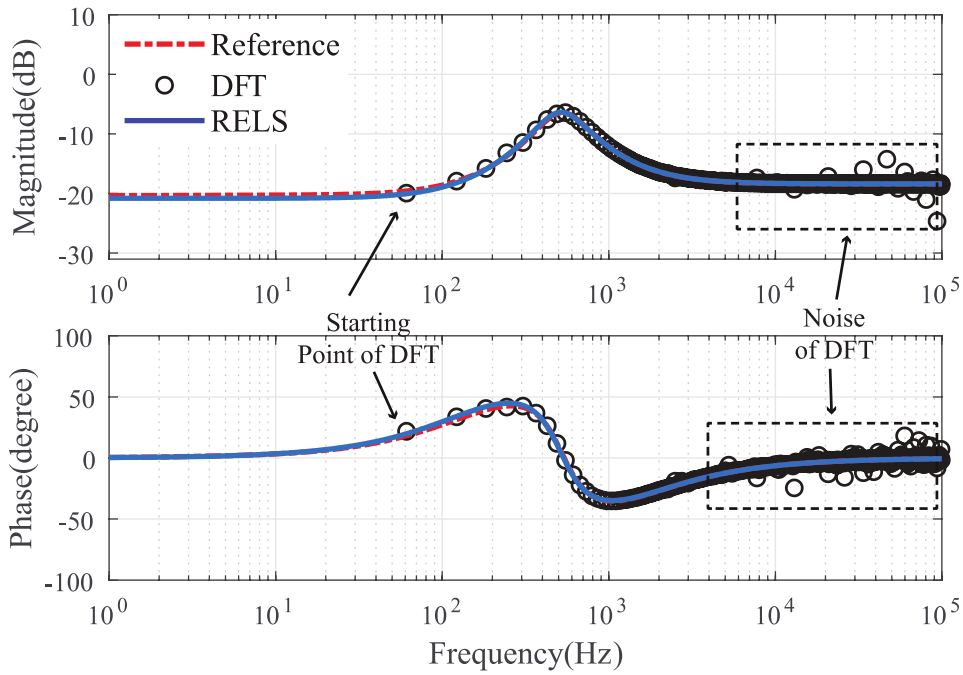

Figure 3. 7 Bode plots of source output impedance obtained using the subject impedance estimation methods for Case 1.

3.3.1.2 Case 2: Simulation with Noise

Next, to emulate a more practical test in the real environment, the white noise of 0.3% p.u. is added to current and 0.5% to the voltage measurements, and the sampling rate is changed to 10 kHz. Figure 3. 8 shows the transient response of the current and voltage under the perturbation test. In this case, the ARMAX model order is set as n_a=6, n_b=6, n_c=1, where the model order is increased to more accurately represent the system considering noise. The parameter vector $\boldsymbol{\theta}(0)$ is set as zero vector, and the covariance $\mathbf{P}(0) = 10^8\mathbf{I}_{14}$. Moreover, as noted in Sections 1.2.1 and 2.2.1.2, to increase noise tolerance in the high frequency range, the last seven data points of $\Delta v(k)$ and $\Delta i(k)$ are measured for RELS algorithm to cover the first overshoot in the transient (e.g., from 0 to 0.6 ms).

After applying the RELS algorithm and eliminating two pairs of unnecessary complex poles and two pairs of complex zeros in the high frequency, the transfer function is calculated as,

$$Z_{RELS\_Case2}(z^{-1}) = \frac{0.1938 - 0.2643z^{-1} + 0.0799z^{-2}}{1 - 1.6390z^{-1} + 0.7420z^{-2}}. \tag{3.16}$$

The Bode plots of the source output impedance for Case 2 are shown in Figure 3. 9. As seen in Figure 3. 9, the DFT method, despite attaining sensible frequency response in the low frequency range from 77.52 Hz to 1000 Hz, shows spurious results in the high frequencies. On the contrary, the results of the RELS method are generally consistent with the reference solution in the entire range of 1 to 5000 Hz. It is also noted that the RELS results show some small error in the high frequency range (starting from 500 Hz), which is due to the limitation of the sampling rate (i.e., 10 kHz for Case 2). This is expected since the accuracy of impedance measurement (regardless of the parameter estimation method) would be compromised due to the reduced sampling rate,

especially in the high frequencies. This loss of accuracy can be avoided by increasing the measurement sampling rate.

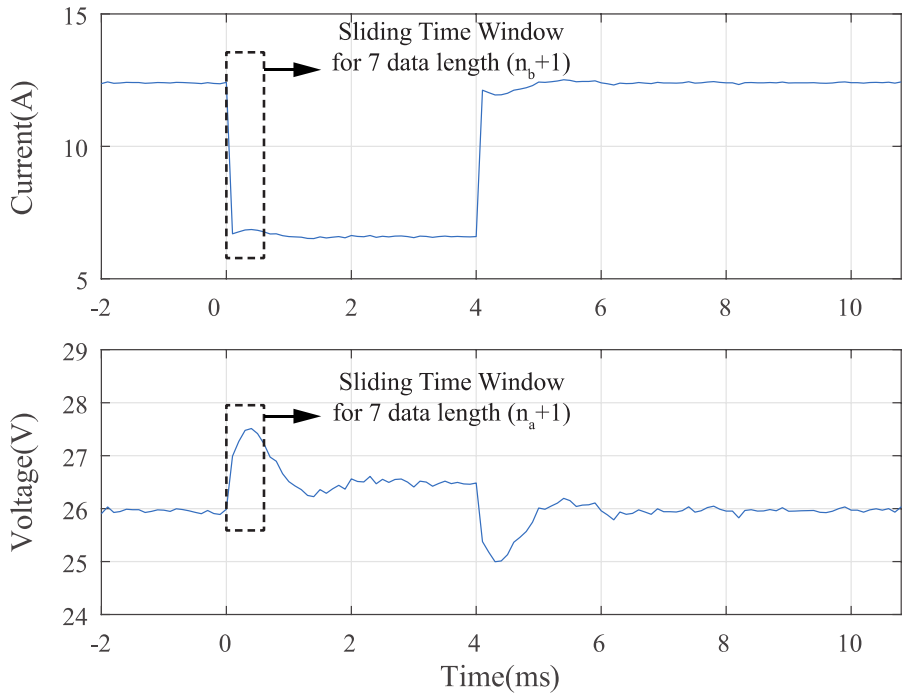

Figure 3. 8 Transient response of current and voltage for Case 2 under the perturbation test.

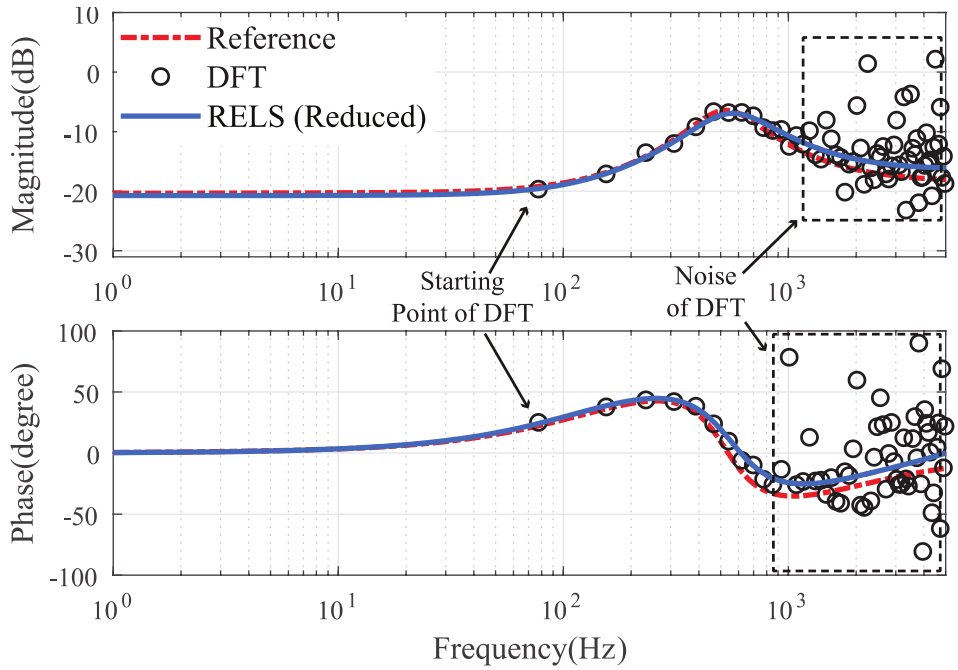

Figure 3. 9 Bode plots of source output impedance obtained using the subject impedance estimation methods for Case 2.

3.3.1.3 Case 3: Experiment Test

To further validate the effectiveness of the proposed RELS method, an experiment test has been carried out for source impedance estimation with the system shown in Figure 3. 3, where the switch is implemented using a gate driver connected to a microcontroller. The initial settings for the RELS algorithm remain the same as those for Case 2.

Figure 3. 10 shows the transient response of the measured voltage (relative error 0.3%) and current (relative error: 0.5%) with a sampling rate of 10 kHz. The final transfer function is obtained as

$$Z_{RELS\_Case3}(z^{-1}) = \frac{0.1660 - 0.1991z^{-1} + 0.0434z^{-2}}{1 - 1.6460z^{-1} + 0.7473z^{-2}}. \tag{3.17}$$

The Bode plot of the source output impedance is shown in Figure 3. 11. Therein, similar to Case 2, the DFT method solution starts to diverge after 1000 Hz, resulting in significant noise in the high frequency range. It is also seen in that the RELS method yields frequency response that is consistent with the reference solution in the entire range of 1 to 5000 Hz, without any noticeable error. This experimental test validates the previous simulation results.

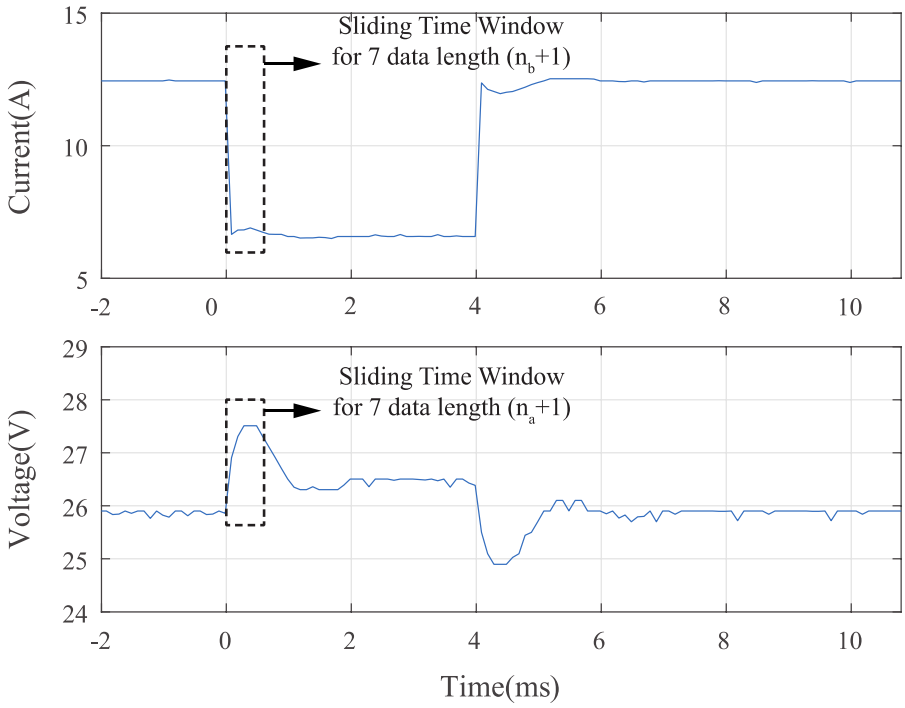

Figure 3. 10 Transient response of current and voltage for Case 3 under the perturbation test.

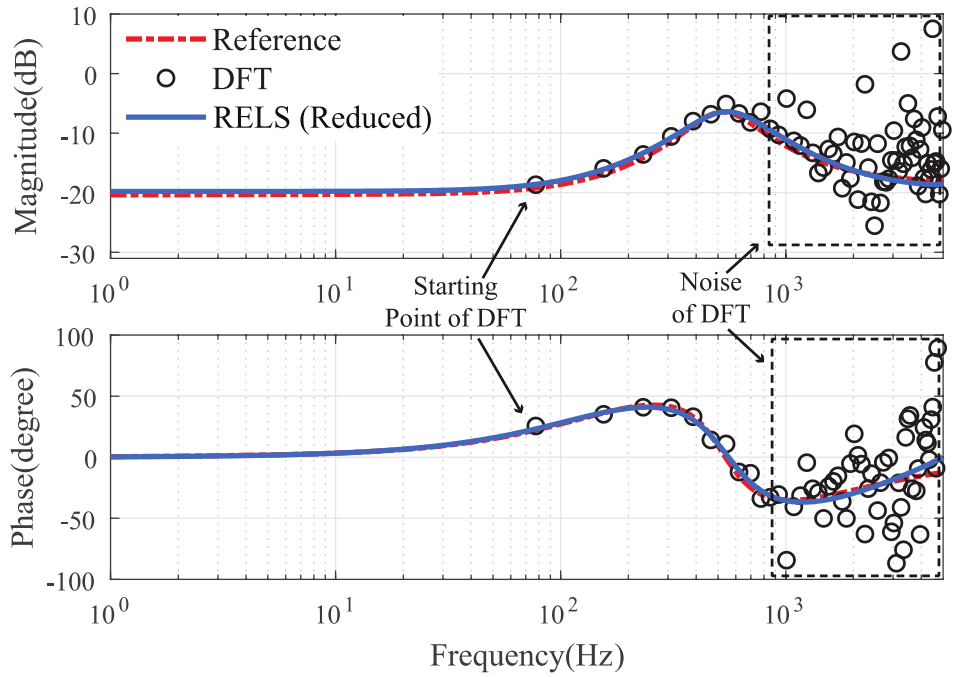

Figure 3. 11 Bode plots of source output impedance obtained using the subject impedance estimation methods for Case 3.

3.3.1.4 Order Reduction

To demonstrate the procedure of order reduction, Case 3 is analyzed for example. In this case, the estimator firstly obtains the impedance transfer function of 6th order,

$$Z_{RELS\_6th}(z^{-1}) = \frac{0.1721 + 0.0259z^{-1} - 0.0297z^{-2} - 0.0676z^{-3} - 0.0412z^{-4} - 0.0231z^{-5} + 0.0117z^{-6}}{1 - 0.2801z^{-1} - 0.2574z^{-2} - 0.2683z^{-3} - 0.0619z^{-4} + 0.1423z^{-5} + 0.1930z^{-6}} \quad . \tag{3.18}$$

For (3.18), its frequency response is illustrated in blue lines in Figure 3. 12, poles and zeros listed in Table 3. 2, and dc gain is 0.1029. It is noted that this full-order transfer function (3.18) has two unnecessary pairs of complex poles and two unnecessary pairs of complex zeros (shown in the last four rows of Table 3. 2), which are produced by the noise (illustrated in the callout in Figure 3. 12) and can be eliminated. After eliminating unnecessary poles and zeros, the selected poles and zeros

(highlighted in Table 3. 2) and the obtained dc gain are used to reconstruct the reduced-order transfer function as (3.17) using (3.12) and (3.13). The frequency response of reconstructed impedance transfer function is illustrated in orange line in Figure 3. 12.

Hereafter in this thesis, the order reduction technique as demonstrated here is applied to all the cases which consider the measurement noise, and will not be illustrated in detail for simplicity.

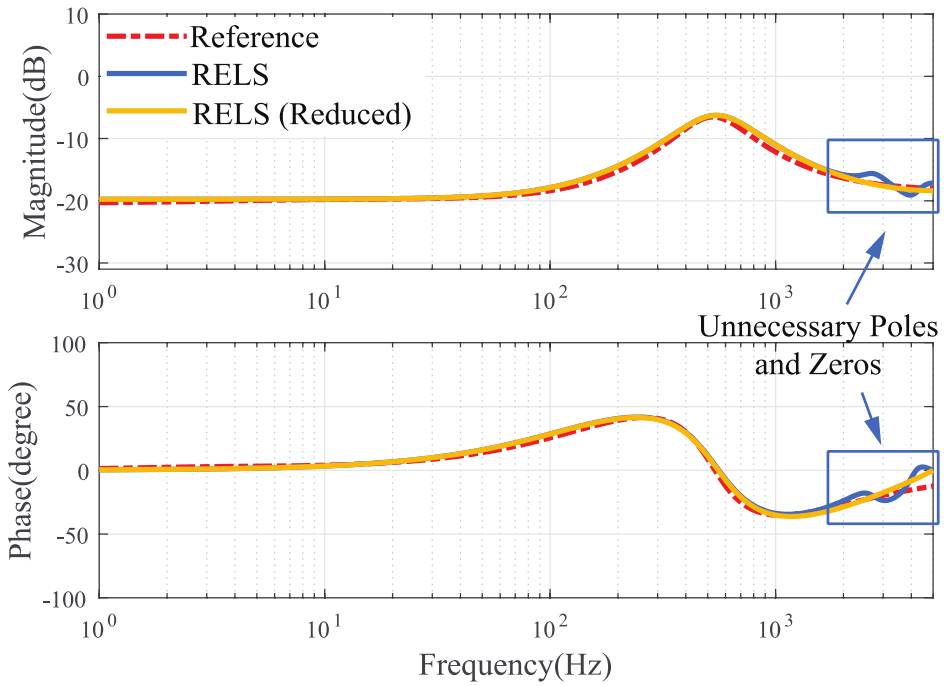

Figure 3. 12 Frequency response comparison between full-order transfer function and reduced-order impedance for Case 3.

Table 3. 2 Poles and zeros of full-order estimated impedance for Case 3.

Poles	Zeros
0.8231+0.2641j	**0.9122**
0.8231-0.2641j	**0.2868**
-0.0936+0.7508j	-0.6061+0.3919j
-0.0936-0.7508j	-0.6061-0.3919j
-0.5895+0.3221j	-0.0685+0.7015j
-0.5895-0.3221j	-0.0685-0.7015j

3.3.1.5 Numerical Properties of Algorithms

To further demonstrate the advantages of the RELS method, the numerical assessment of the subject methods is summarized in Table 3. 3. Therein, for Case 1 (i.e., ideal case without noise), the DFT method stores two vectors of $\Delta\mathbf{v}$ and $\Delta\mathbf{i}$ with the length of 16384 points each, yet the RELS method only needs to store the last three data of $\Delta\mathbf{v}$ and $\Delta\mathbf{i}$. As a result, the DFT method can only calculate results after recording the whole transient response (i.e., from 0 to 16.383 ms), while the RELS method iteratively updates the results on-the-fly, which converges after 0.218 ms (i.e., 219 data points). Moreover, for Cases 2 and 3 where the noise in the system is considered, the advantages of the RELS method are also validated over the DFT method with shorter stored vector length and sampled transient period as seen in Table 3. 3.

Table 3. 3 Numerical properties of the subject impedance estimation methods for scenario 1.

		DFT		RELS	
Case	**Sampling Rate**	**Stored Vector Length**	**Sampled Transient Period (ms)**	**Stored Vector Length**	**Sampled Transient Period (ms)**
1	1 MHz	16384	16.383	3	0.218
2	10 kHz	128	12.8	7	2
3	10 kHz	128	12.8	7	3.3

As seen in Table 3. 3, to calculate the frequency response, the DFT method requires to store all the measured $\Delta\mathbf{v}$ and $\Delta\mathbf{i}$ for the entire transient response, whereas the RELS method only requires the last few sampled data points to form a sliding time window. The length of the time window is determined by the order of the ARMAX model.

3.3.1.6 System Parameters Estimation

Finally, the system parameters for the above three cases based on RELS are calculated using (3.5) as listed in Table 3. 4. The estimated parameters for all the three cases match well with the actual values. It is also noted that the estimation of R_d is affected by the system noise appearing at the first overshoot, and the calculation of L_{tl} and C_d are based on the value of R_d. As a result, for Cases 2 and 3, the estimated R_d, L_{tl} and C_d can be slightly different from their actual values. These estimated results can be further applied to the adaptive controller design.

Table 3. 4 Estimated parameters of the considered system for scenario 1.

		Rl (Ω)	Rd (Ω)	Ltl (μH)	Cd (mF)
Actual Value		**0.096**	**0.120**	**92.000**	**1.000**
Estimated Value	**Case 1**	0.091	0.121	90.001	1.064
	Case 2	0.092	0.193	95.701	0.867
	Case 3	0.103	0.163	89.742	0.938

3.3.1.7 Remarks

In summary of Scenario 1, we propose a new method for online estimation of the source impedance in dc distribution systems. The method is implemented through RELS analysis of the system transient response after applying an impulse injection. Compared with the established DFT method, the proposed RELS method features benefits of the direct parametric solution, better resilience to noise in the high frequency range, and lower requirement on data memory and processing time. Therefore, this method can become a feasible tool for interconnection of stabilizers and adaptive controllers in future dc distribution systems.

3.3.2 Scenario 2: impedance estimation based on RELS algorithm while using impulse and PRBS injections

In Scenario 1, the simulation studies and experimental test are carried out for the dc distribution system with a passive load. However, in practice, the dc distribution system can be connected to active loads (e.g., power electronic devices) that has complex profiles of impedance spectrum due to harmonics, noises, etc.

In Scenario 2, the considered dc system (illustrated in Figure 3. 3) is loaded with a buck converter regulated by its output voltage, whose detailed parameters are listed in Appendix C. In addition, to have less influence on the system stability, another injection—PRBS injection is introduced. Both impulse injection and PRBS injection are implemented by adding the impulse signal or PRBS signal into the reference voltage of the buck converter. The impedance estimation based on the proposed RELS algorithm is tested using the impulse and PRBS injections, as summarized in Table 3. 1. Specifically, two case studies are performed: 1) Case 4: Simulation without measurement noise and using a) impulse and b) PRBS injections; 2) Case 5: Simulation with measurement noise and using a) impulse and b) PRBS injections.

3.3.2.1 Case 4: Simulation without Measurement Noise

3.3.2.1.1 Case 4a: Impulse Injection

Firstly, the proposed RELS algorithm is tested on an ideal system (without measurement noise) using impulse injection. In this test, an impulse signal (-8V) is added to the reference voltage of buck converter (initially 20V) for a time duration period of 2 ms. The transient response of the system under the impulse injection is shown in Figure 3. 13, where the sampling rate for measured $\Delta i(k)$ and $\Delta v(k)$ is 10 kHz. The initial settings for the proposed RELS algorithm are as follows: the

ARMAX model order is set as n_a=6, n_b=6, n_c=1, the parameter vector $\boldsymbol{\theta}(0)$ is set as a zero vector, and the covariance $\mathbf{P}(0) = 10^4\mathbf{I}_{14}$.

To evaluate the accuracy of the predicted results, the two-norm error of the obtained frequency response is calculated as

$$\varepsilon(Z_{RELS}) = \frac{\left\| Z_{RELS} - Z_{ref} \right\|_2}{\left\| Z_{ref} \right\|_2} \times 100\% \tag{3.19}$$

Here, Z_{RELS} denotes the RELS obtained frequency response from the impedance with reduced order, and Z_{ref} denotes the reference frequency response. In the following cases, two-norm error is calculated respectively for the obtained frequency response to assess the performance of the obtained results.

After applying the RELS algorithm and eliminating two pairs of unnecessary complex poles and two pairs of unnecessary complex zeros in the high frequency, the transfer function is calculated as

$$Z_{RELS\_Case4a}(z^{-1}) = \frac{0.1640 - 0.2184z^{-1} + 0.0636z^{-2}}{1 - 1.6940z^{-1} + 0.7902z^{-2}}. \tag{3.20}$$

The Bode plots of the source output impedance obtained using the subject impedance estimation methods are shown in Figure 3. 14. As seen in Figure 3. 14, the DFT method starts to attain the frequency response from 39 Hz and shows noise in the high frequency range (over 3 kHz). At the same time, the RELS method yields frequency response that is consistent with the reference solution in the entire range, and the two-norm error of the frequency response produced by RELS (Reduced) is 0.26% compared to reference solution. This validates the advantageous accuracy of the RELS method over the DFT method.

However, it is noted in Figure 3. 13 that, the impulse injection causes the converter input current to dip during transient, reaching a minimum value of around 3 A. This significantly influences the stability of the interconnection and can trigger the protection circuit of the converter system. Once triggered, the protection circuit will also change the converter switching pattern, thus affecting the impedance of source and making the estimated results inaccurate.

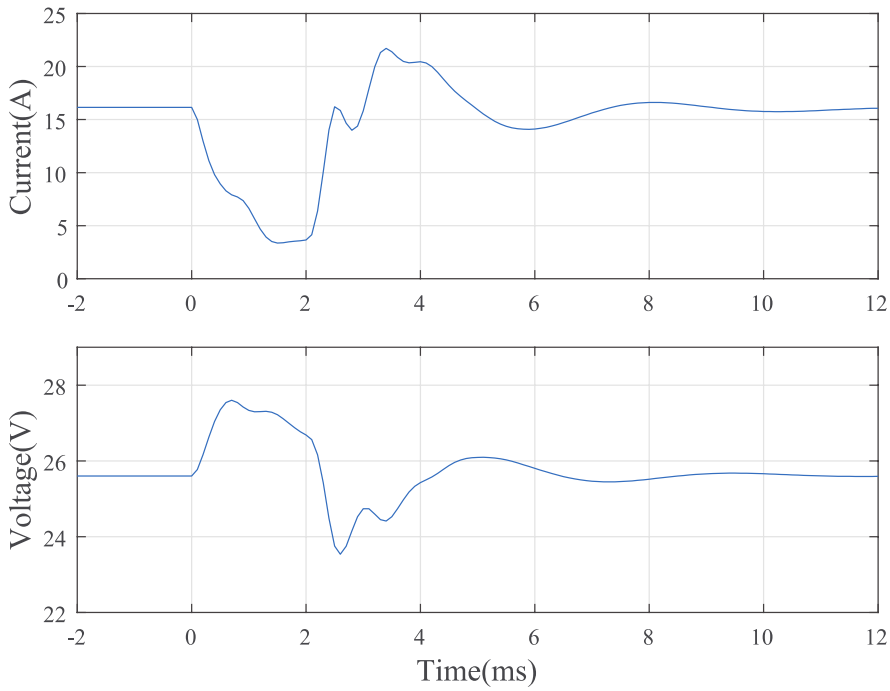

Figure 3. 13 Transient response of current and voltage for Case 4a under the impulse injection.

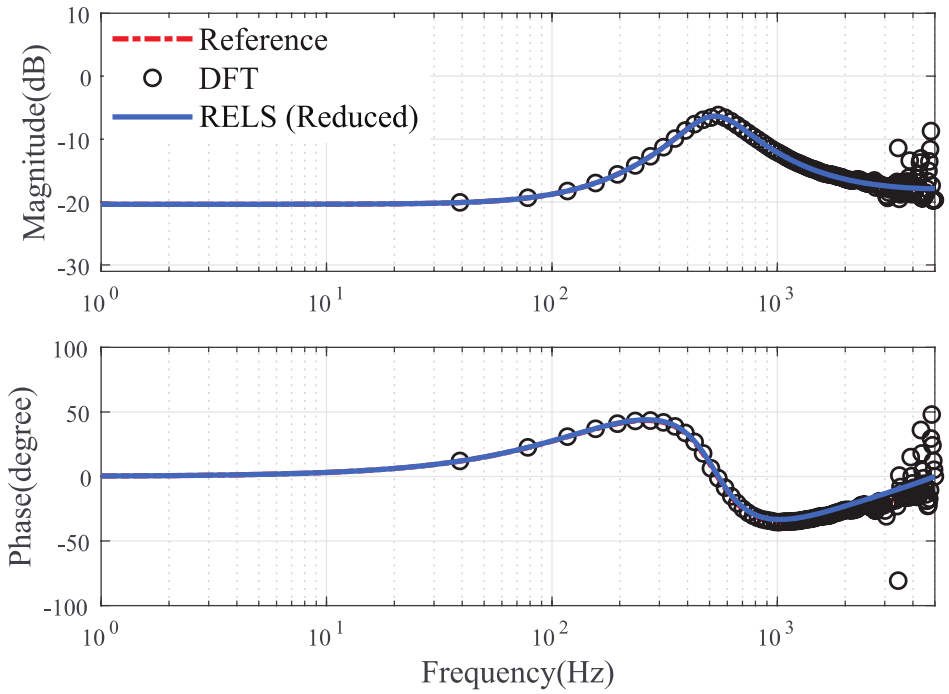

Figure 3. 14 Bode plots of source output impedance obtained using the subject impedance estimation methods for Case 4a.

3.3.2.1.2 Case 4b: PRBS Injection

To avoid influence of signal injection on the system stability, another injection—PRBS injection is tested in Case 4b. Instead of using impulse injection, PRBS signal with 250 data points with 10 Samples/ms are added to the reference voltage of buck converter, with magnitude of 2V or -2V and a duration period of 25 ms. The transient response of the system under the PRBS injection is shown in Figure 3. 15, where the sampling rate for measurements and the RELS initial settings remains same as Case 4a.

The obtained transfer function is calculated as,

$$Z_{RELS\_Case4b}(z^{-1}) = \frac{0.1637 - 0.2177z^{-1} + 0.0633z^{-2}}{1 - 1.6940z^{-1} + 0.7903z^{-2}}. \tag{3.21}$$

The Bode plots of the source output impedance obtained using the subject impedance estimation methods are shown in Figure 3. 16. As seen in Figure 3. 16, the obtained frequency response using

DFT method shows worse accuracy than Case 4a in the high frequency range (over 800 Hz), which indicates that PRBS injection is not suitable for DFT analysis. At the same time, the frequency response of RELS is consistent with the reference solution in the entire range, and two-norm error of the frequency response produced by RELS (Reduced) is 0.21% compared to reference solution. Moreover, it is noted in Figure 3. 16 that, with PRBS injection, the converter input current will not dip significantly during transients. This verifies the advantages of impedance estimation based on RELS algorithm while using PRBS injection.

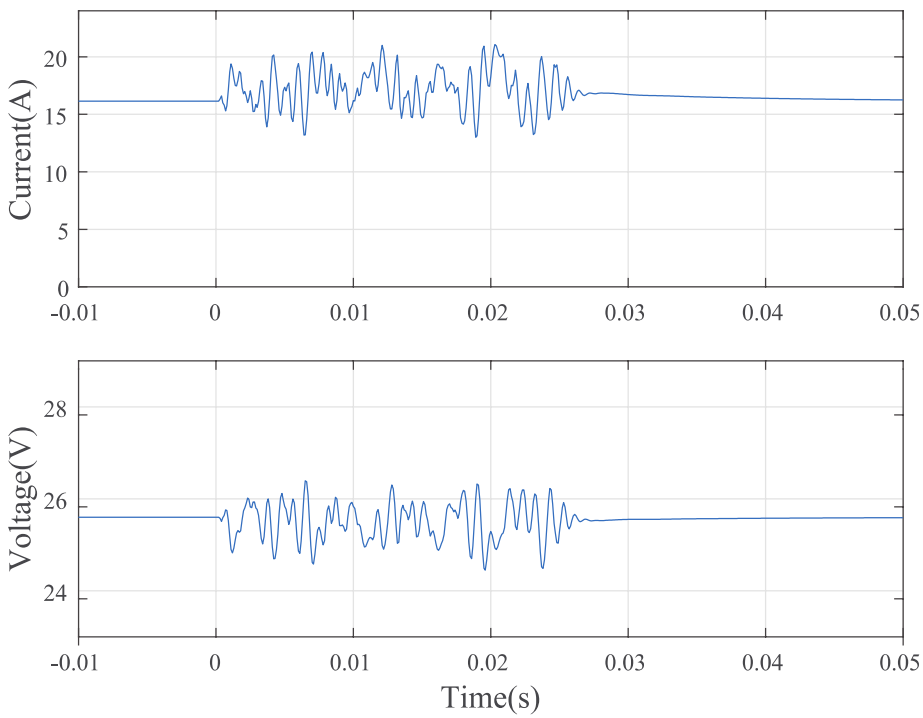

Figure 3. 15 Transient response of current and voltage for Case 4b under the PRBS injection.

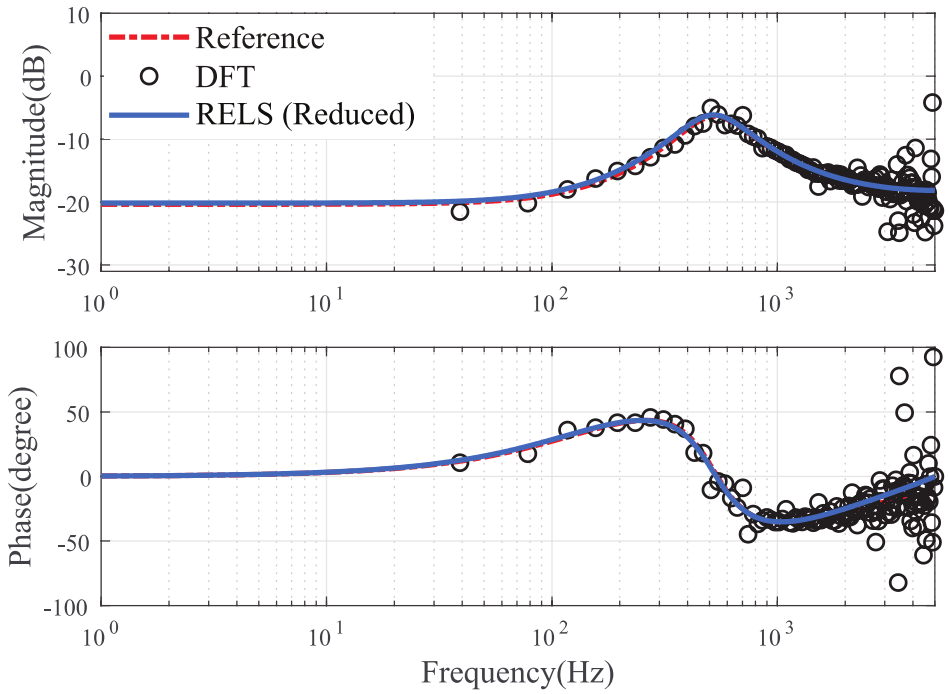

Figure 3. 16 Bode plots of source output impedance obtained using the subject impedance estimation methods for Case 4b.

3.3.2.2 Case 5: Simulation with Measurement Noise under Impulse (Case 5a) vs. PRBS Injection (Case 5b)

Next, to emulate a more practical test, the white noise of 1.0% p.u. is added to the current and voltage measurements, and the sampling rate remains as 10 kHz. Figure 3. 17 shows the transient response of the current and voltage with measurement noise under impulse injection (Case 5a), while Figure 3. 18 shows those under PRBS injection (Case 5b). In both cases, the ARMAX model order is set as n_a=6, n_b=6, n_c=1. The parameter vector $\boldsymbol{\theta}(0)$ is set as zero vector, and the covariance $\mathbf{P}(0) = 10^4\mathbf{I}_{14}$.

The obtained reduced-order transfer functions are calculated in discrete-time domain for both signal injections as,

$$Z_{RELS\_Case5a}(z^{-1}) = \frac{0.1629 - 0.2042z^{-1} + 0.05145z^{-2}}{1 - 1.6750z^{-1} + 0.7777z^{-2}}, \tag{3.22}$$

$$Z_{RELS\_Case5b}(z^{-1}) = \frac{0.1361 - 0.1533z^{-1} + 0.0281z^{-2}}{1 - 1.6480z^{-1} + 0.7541z^{-2}}. \tag{3.23}$$

The Bode plots of the estimated source output impedance for Case 5a and 5b are shown in Figure 3. 19. Since RELS has been verified more advantageous over DFT method in Case 4a and 4b, the DFT results are not illustrated here. The two-norm error of frequency response are calculated: 2.10% for Case 5a and 2.82% for Case 5b, which show that both results are generally consistent with the reference solution in the range of 1 to 5000 Hz.

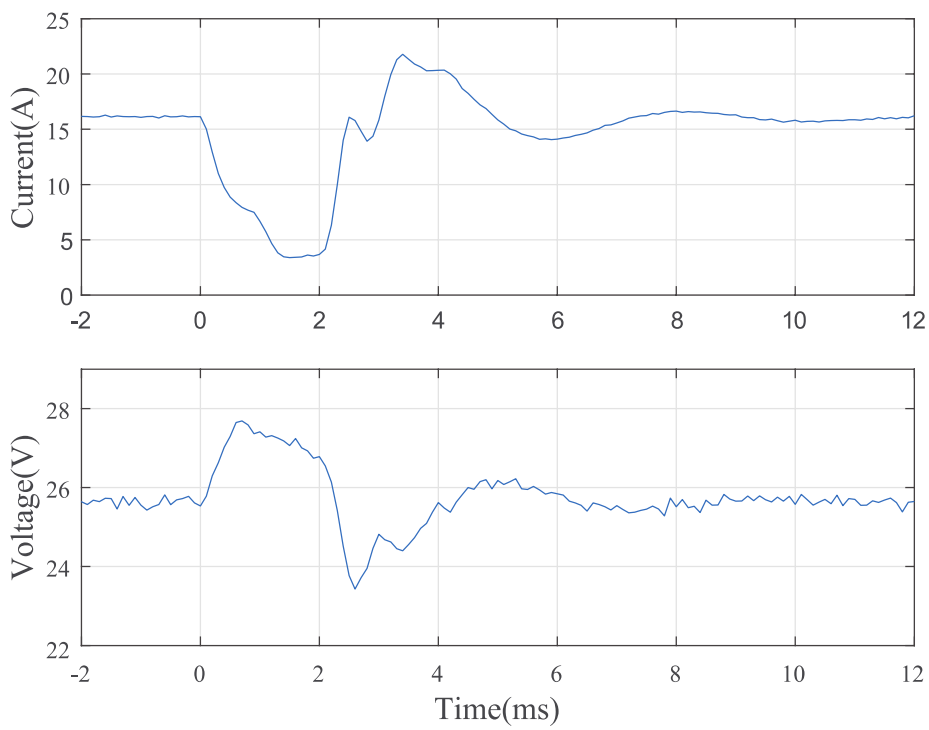

Figure 3. 17 Transient response of current and voltage under the impulse injection (Case 5b).

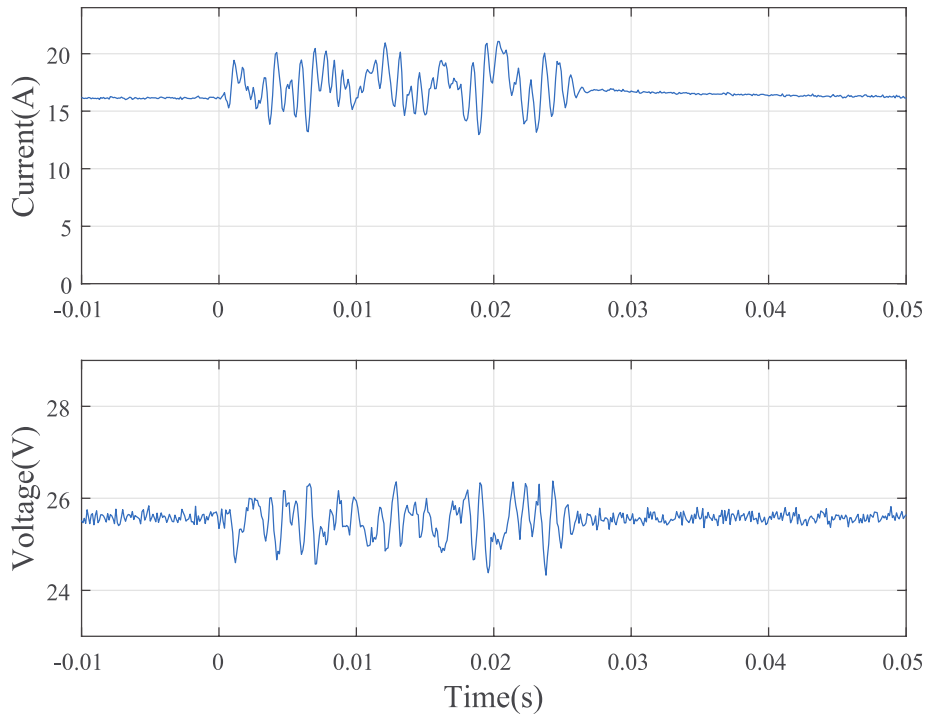

Figure 3. 18 Transient response of current and voltage under the PRBS injection (Case 5b).

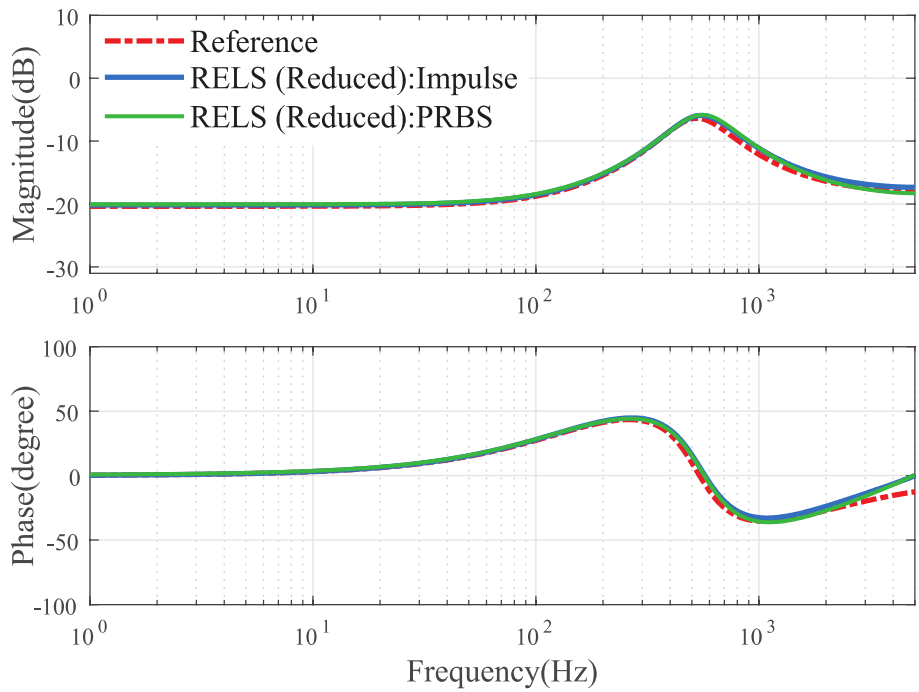

Figure 3. 19 Bode plots of source output impedance obtained using the RELS estimation method under impulse injection (Case 5a) and PRBS injection (Case 5b).

3.3.2.3 Numerical Properties of Algorithms

The numerical assessment of the subject impedance estimation for Case 4 and Case 5 are listed in Table 3. 5, where the RELS method is shown with numerical advantages over the DFT method. For the requirement of stored date, the DFT method need to store two vectors of $\Delta\mathbf{v}$ and $\Delta\mathbf{i}$ with the length of 256 points each, while the RELS method only needs to store the last seven data of $\Delta\mathbf{v}$ and $\Delta\mathbf{i}$. In addition, the RELS method with impulse injection requires less samples than that with PRBS injection.

Table 3. 5 Numerical properties of the subject impedance estimation methods for scenario 2.

		DFT		RELS	
Case	**Injection Signals**	**Stored Vector Length**	**Sampled Transient Period (ms)**	**Stored Vector Length**	**Sampled Transient Period (ms)**
4a	Impulse	256	25.6	7	4.5
4b	PRBS			7	25
5a	Impulse			7	10
5b	PRBS			7	25

As also seen in Table 3. 5, the sampled transient periods required by RELS method using impulse and PRBS injections are both shorter than that of DFT method (25.6 ms). Specially, for impulse injection (i.e., Case 4a, 5a in Table 3. 5), compared with Table 3. 3 (i.e. Case 2, 3), the required sampled transient period for estimated parameters convergence increases into 10-25 ms due to the complexity of the load. It is worth mentioning that, because of the measurement noise, the accuracy of estimation results will be influenced by the overflow of the covariance matrix at the end of transients. Therefore, it is necessary to find the time span required for the entire transient and stop the recursive iteration around the end of the time interval when applying the impulse injection. At the same time, for PRBS injection (i.e. Case 4b, 5b in Table 3. 5), the sampled

transient period is determined by the time span of PRBS injection signals. Therefore, the end time of iteration is determined in advance and has to be kept as 25 ms (250 iterations).

3.3.2.4 System Parameters Estimation

The system parameters are calculated using (3.5) and based on the results of RELS method for the above four cases, as listed in Table 3. 6. Therein, the estimated parameters for all the four simulation cases match well with the actual values, with acceptable error. To be more specific, for ideal simulation Case 4a, the relative errors of line resistance R_l, damping resistance R_d, parasitic inductance L_{tl} and passive damping capacitance C_d are 0.08%, 0.68%, 0.24% and 0.66%, respectively; and for Case 4b, the relative errors are 0.02%, 1.03%, 0.65% and 0.83%, respectively. For the two simulation cases with measurement noise (5a, 5b), the relative errors of line resistor R_l, damping resistor R_d, parasitic inductor L_{tl} and passive damping capacitor C_d are respectively 3.13%, 8.77%, 10.02% and 2.94% for Case 5a; and for Case 5b, the relative errors are 3.13%, 8.33%, 12.19% and 0.8%, respectively. This loss of accuracy is caused by limitation of the measurement sampling rate. These estimated results obtained from the RELS method are considered acceptable for applications in the adaptive controller design.

Table 3. 6 Estimated parameters of the considered system for scenario 2.

		R_l (Ω)	R_d (Ω)	L_{tl} (μH)	C_d (mF)
Actual Value		**0.096**	**0.120**	**92.000**	**1.000**
Estimated Value	**Case 4a**	0.096	0.119	91.392	1.002
	Case 4b	0.096	0.119	91.234	1.006
	Case 5a	0.099	0.109	82.774	1.029
	Case 5a	0.099	0.110	80.778	1.008

3.3.2.5 Noise Tolerance and Order Selections

To compare the performance of impulse injection and PRBS injection, the same system is tested with the impedance transfer function order ranging from 2nd to 10th, and the relative error of measurements ranging from 0.1% to 4.0%. The two-norm error of estimation results are listed in Table 3. 7

As can be observed in Table 3. 7, the RELS algorithm using both injections generally has the satisfactory noise tolerance. The accuracy of estimation for each injection is decreased with larger relative error and decreased order selections. Specifically, the estimation results for 2nd order and 4th order are inaccurate when the relative error of measurement is larger than 0.1%; while those for 6th, 8th and 10th orders achieve the accurate results, among which, 6th order (marked in orange) achieves the best estimation results with both injection types.

Table 3. 7 Two-norm error results of bode plots comparison.

Relative Error of Measurements (%)		0.1	0.5	1.0	1.5	2.0	2.5	3.0	3.5	4.0
Impulse Injection										
Order Selection	**2nd**	3.56	--	--	--	--	--	--	`--	--
	4th	1.77	4.33	--	--	--	--	--	--	--
	6th	1.34	2.40	2.10	4.06	4.57	4.20	4.41	4.76	5.11
	8th	1.23	5.38	9.39	6.58	6.20	5.84	6.55	6.47	6.87
	10th	0.71	5.32	6.77	5.38	6.01	7.08	7.44	7.02	6.56
PRBS Injection										
Order Selection	**2nd**	3.41	--	--	--	--	--	--	--	--
	4th	0.60	3.54	--	--	--	--	--	--	--
	6th	0.65	1.85	2.82	3.47	3.82	3.83	4.18	4.56	5.14
	8th	1.07	4.64	2.90	5.95	7.40	6.94	7.58	7.83	8.47
	10th	0.40	2.10	2.15	3.32	7.57	6.96	7.09	6.79	6.71

3.3.2.6 Remarks

In Scenario 2, the proposed RELS method is tested based on the system transient response after applying an impulse or PRBS injections. From above four cases, the RELS method demonstrates the advantages over DFT method with direct parametric solution, lower memory requirement for stored data and smaller processing time, and higher noise tolerance. In addition, it is noted that PRBS injection has less influence on system stability, while requiring more complex signal storage and longer injection time compared with impulse injection. For accuracy of parameter estimation, both injection methods show similar results applying the RELS algorithm.

However, in the actual measurement, the way to improve the accuracy of estimation is through increasing the effective duration of transients, which will significantly influence the stability of system while using impulse injection, or will require longer time duration while using PRBS injection (25 ms for Scenario 2).

Chapter 4: Implementation of Online Source Impedance Estimation on HIL Platform

To further verify the feasibility and effectiveness of the proposed impedance estimation method in real-time applications, two HIL experimental tests are carried out: 1) Case 6a: impedance estimation under impulse injection based on HIL experiment (verification of Case 5a); 2) Case 6b: impedance estimation under PRBS injection based on HIL experiment (verification of Case 5b).

4.1 HIL Experiment Platform

The HIL experimental test is carried based on OPAL-RT real-time simulator OP5700 platform, and the DSP TMS320F28335. During the HIL experiment, the dc distribution system loaded with a buck converter as illustrated in Figure 3. 3 is implemented in MATLAB/Simulink and simulated in OP5700, the SCADA interface is designed in LabVIEW and the impedance measurement is implemented in the TMS320F28335. Figure 4. 1 briefly illustrates the connection among the tested subsystems, SCADA interface, and DSP.

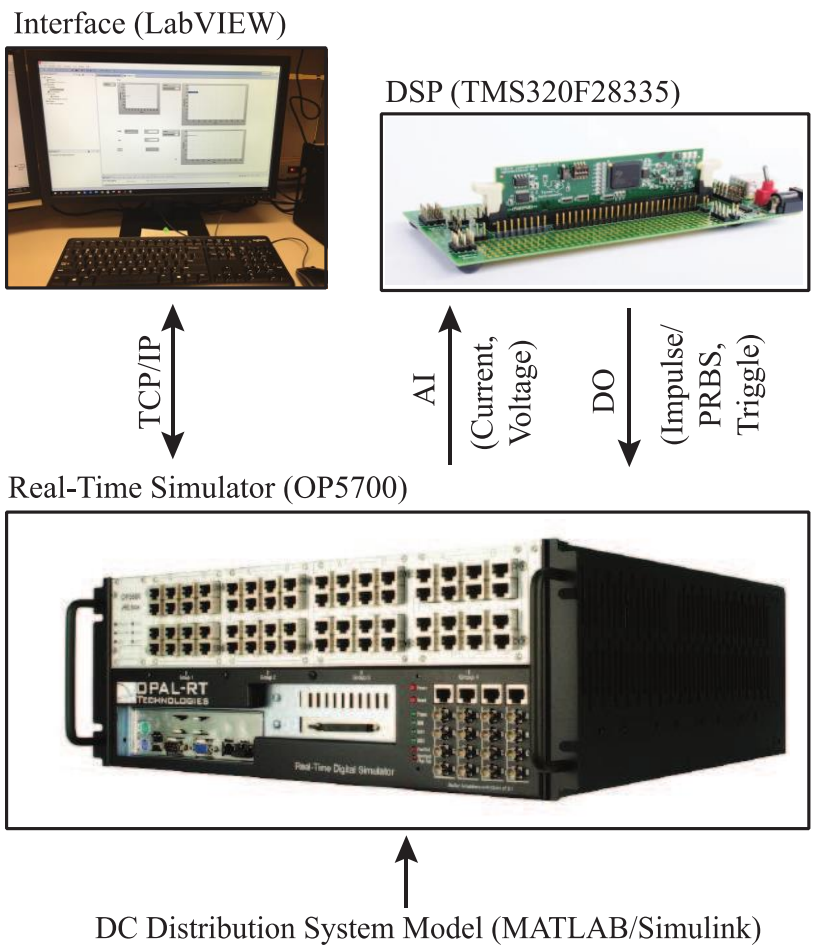

Figure 4. 1 Overview of the HIL experiment system for impedance measurement.

4.2 Case 6: HIL Experiment under Impulse (Case 6a) vs. PRBS Injection (Case 6b)

To demonstrate the process of the proposed online impedance estimation on HIL platform, an example (i.e., Case 6a: impedance estimation under impulse injection based on HIL experiment) is demonstrated in conjunction with Figure 4. 2, which depicts the time allocation of the tasks performed by the DSP. The initial setting for RELS algorithm in DSP are T_s=10^{-4}s, n_a=6, n_b=6, n_c=1, $\boldsymbol{\theta}(0)$ is set as zero vector, and the covariance $\mathbf{P}(0)$ =$10^4\mathbf{I}_{14}$; the time step for real-time simulator is 10^{-5} s; the DSP sampling rate is 10 kHz; and the measurement noise of voltage and current are 0.6% and 1.1%, respectively.

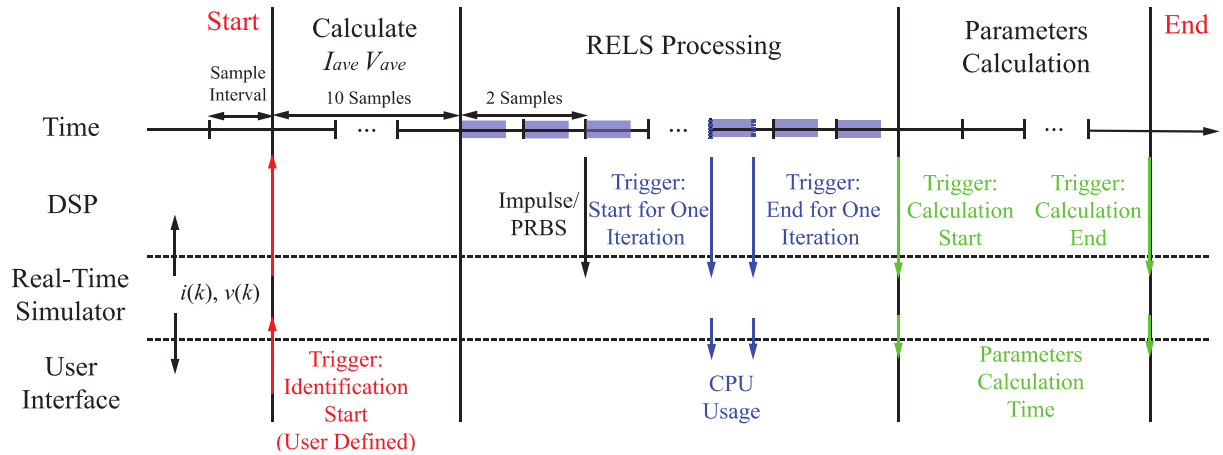

Figure 4. 2 Time allocation of HIL experiment.

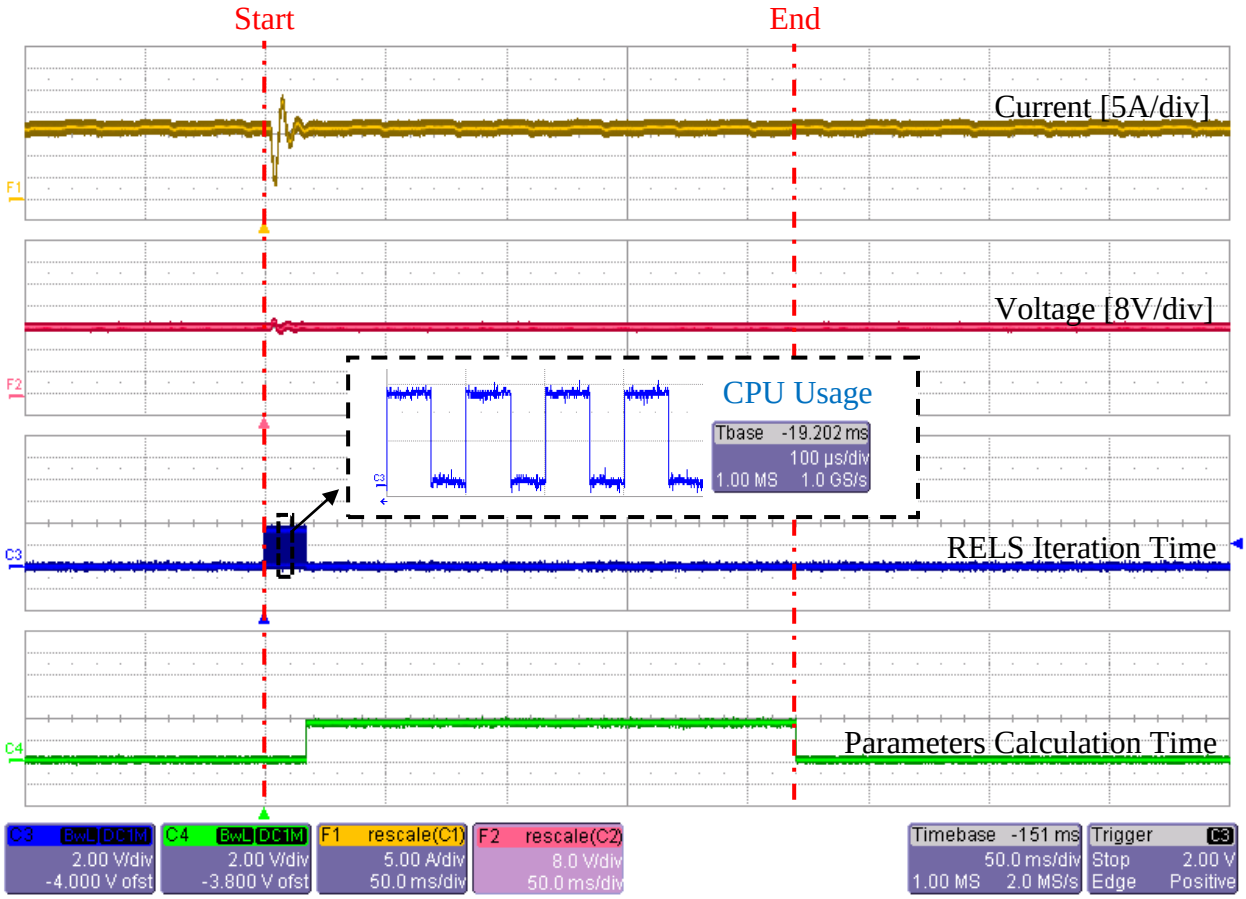

Figure 4. 3 DSP implementation for Case 6a with impulse injection with order selection of n_a=6, n_b=6, n_c=1.

Figure 4. 3 illustrates the signals captured from oscilloscope, which are the same as the figures shown in the SCADA interface in LabVIEW. As illustrated in Figure 4. 2 and seen in Figure 4. 3, when the user starts the impedance estimation process in the SCADA interface, the real-time simulator receives the trigger signal through TCP/IP and generates a digital signal to DSP immediately. The DSP then calculates the average values of current and voltage (using 10 sample periods), which are used to calculate the small-signal values for the RELS algorithm. Next, the estimator uses two iterations for initialization, and injects an impulse signal into the voltage reference of the buck converter, from then the estimator runs the RELS algorithm for impedance estimation iteratively while the HIL simulation runs simultaneously. This process is set to terminate after 170 iterations to avoid the wind-up of estimated results. Finally, the RELS estimation results are used to reconstruct the transfer function of impedance and calculate the parameters of source system. For Figure 4. 3, the CPU usage is 55.8%, and total estimation time (including the time for calculating the average values and for RELS processing) is 0.0180s, and the parameter calculation time is 0.2031s (marked in green) [which is relatively long due to use of Durand-Kerner method, as recalled in Section2.2.1.3]. The total processing time for the RELS-based impedance estimation using impulse injection is 0.2211 s.

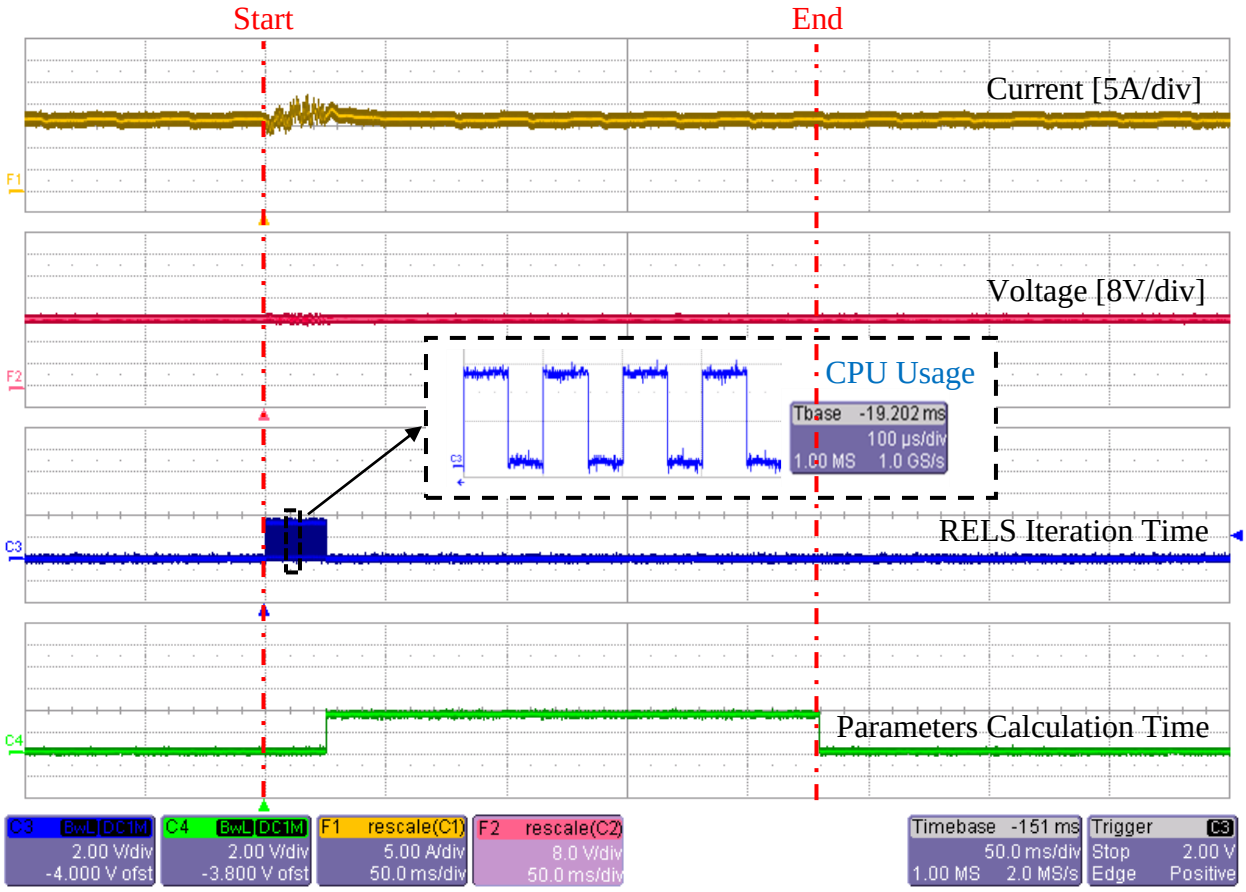

Figure 4. 4 DSP implementation for Case 6b with PRBS injection with order selection of n_a=6, n_b=6, n_c=1.

Similarly, the results of HIL experimental test Case 6b are presented: impedance estimation under PRBS injection (verification for Case 5b) are shown in Figure 4. 4. The initial settings are the same as Case 6a, and the parameter estimation follows the same procedure as illustrated in Figure 4. 2, except that this time the system is injected with 250 PRBS signals (this value can be decreased if needed) that are pre-stored in DSP. As seen in Figure 4. 4, the CPU usage is 55.8%, and total estimation time (including the time for calculating the average values and for RELS processing) is 0.0260s, and the parameter calculation time is 0.2031s. The total processing time for the RELS-based impedance estimation using PRBS injection is 0.2291 s.

The final transfer functions extracted from DSP are as follow,

$$Z_{RELS\_Case6a}(z^{-1}) = \frac{0.1887 - 0.2569z^{-1} + 0.0761z^{-2}}{1 - 1.6450z^{-1} + 0.7394z^{-2}}, \tag{4.1}$$

$$Z_{RELS\_Case6b}(z^{-1}) = \frac{0.1834 - 0.2616z^{-1} + 0.0869z^{-2}}{1 - 1.7021z^{-1} + 0.7911z^{-2}}. \tag{4.2}$$

The Bode plots of the source output impedance for Cases 6a, 6b are shown in Figure 4. 5. As seen in Figure 4. 5, the results of Case 6a show some deviation from reference solution, while the results of Case 6b achieve better consistency with the reference solution in the entire range except for some phase shift over 1000Hz. The two-norm errors of frequency response for the two cases are calculated as: 6.26% for Case 6a and 3.17% for Case 6b. This indicates that PRBS injection can achieve more accurate results than impulse injection in HIL experiments, which is different from the similar accuracy shown in simulation studies in Section 3.3.2.2.

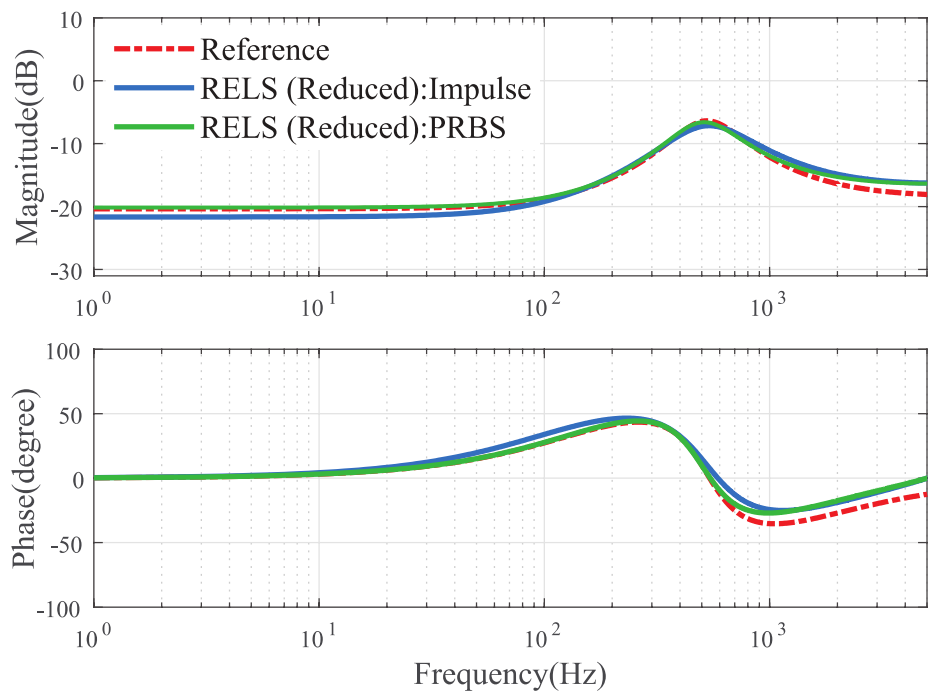

Figure 4. 5 Bode plots of source output impedance obtained using the subject impedance estimation methods for Case 6a and Case 6b.

It is noted in Figure 4. 5 that, the Case 6a magnitude results display more notable deviation from the reference solution in the low frequency range (i.e. 1-100 Hz), as compared to the Case 6b results. This is because the measurement noise in 6a (large-signal injection) is larger than that in 6b (small-signal injection). This not only makes the predicted impedance magnitude to be smaller than actual value in dc gain/low frequencies, but also causes the relatively large error (in both impedance magnitude and phase) in the high frequency range. Another factor affecting the impedance estimation in the high frequency range is the fixed simulation time step used in real time simulator, which limits the maximum frequency response that can be accurately measured according to the Nyquist theorem.

4.3 Numerical Properties of Algorithms

The numerical assessment of the impedance estimation for Case 6 are listed in Table 4. 1. Therein, for both impulse and PRBS injections, the RELS method stores two vectors of $\Delta\mathbf{v}$ and $\Delta\mathbf{i}$ with the length of seven points each. The sampled transient period is 15 ms for impulse injection, which is shorter than that of PRBS injection (i.e., 25ms). From the view of processing time required for the RELS algorithm, the impulse injection gives a faster estimation speed than the PRBS injection, which is also consistent with the simulation results shown in Section 3.3.2.3.

Table 4. 1 Properties of the subject impedance estimation methods for different sampling rates.

Case	Injection Signals	Stored Vector Length	Sampled Transient Period (ms)
6(a)	Impulse	7	15
6(b)	PRBS	7	25

4.4 System Parameters Estimation

The parameters of the source system are calculated using (3.5) automatically in DSP, and summarized as listed in Table 4. 2. From Table 4. 2, we can observe that the estimated parameters for Case 6b are closer to the actual values compared with those for Case 6a. The relative errors of line resistor R_l, damping resistor R_d, parasitic inductor L_{tl} and passive damping capacitor C_d are 13.83%, 20.16%, 18.29%, 20.52% for Case 6a; and 2.29%, 21.12%, 12.99%, 4.45% for Case 6b, respectively. Specially, for Case 6a, because the signal generating and sampling delay between current and voltage, the relative error of R_l estimation is relatively large, which accumulates the estimation error of L_{tl} and C_d. However, for Case 6b, the results are generally more accurate. It is also noted that the R_d estimation in both cases is not so accurate, which is due to the noise in measurement in the high frequency range. These errors may be reduced by increasing the sampling rate. These estimated results can be further applied to the adaptive controller design in the DSP.

Table 4. 2 Estimated parameters of the considered system.

Parameters		**R_l (Ω)**	**R_d (Ω)**	**L_{tl} (μH)**	**C_d (mF)**
Actual Value		**0.096**	**0.120**	**92.000**	**1.000**
Estimated Value	**Case 6a**	0.083	0.144	75.169	1.205
	Case 6b	0.098	0.145	103.955	0.955

4.5 Performance of RELS in DSP

One major feature of the RELS method is that it is able to estimate the system impedance online. When implemented in DSP, the performance of RELS algorithm for different order selections is listed in Table 4. 3. It is noticed that, the CPU usage increases rapidly as the transfer function order grows, and reaches 98% of CPU usage when the order selection is set to 8th (i.e.,

maximum value that given DSP can achieve for online estimation under considered sampling rate). This issue can be improved in the future by optimizing the algorithm (to reduce the CPU consumption) or upgrading the DSP with higher computing power. In addition, the detailed processing time for each order selection is listed in Table 4. 3, where the total processing time is shown less than 0.4s. It is worth mentioning that the parameters calculation takes up the majority of total processing time, because the Durand Kerner Method (in Section 2.2.1.3) requires operations in the order of $O(n \cdot d^2)$ for the DSP to calculate the poles and zeros, which is relatively slow.

Therefore, it is concluded from Table 4. 3 that, for DSP hardware TMS320F28335 as applied here, the proper order selected for impedance transfer function is the 6th-order, to allow for CPU usage reserve in case there are some other instructions needed for tuning adaptive controller.

Table 4. 3 DSP performance under different order selection.

Order Selection	4th	6th	8th
CPU Usage	27.6 %	55.8 %	98.0 %
Impulse Injection			
Impedance Calculation Time (s)		0.0180	
Parameters Calculation Time (s)	0.0893	0.2031	0.3634
Total Processing Time (s)	0.1073	0.2211	0.3814
PRBS Injection			
Impedance Calculation Time (s)		0.0260	
Parameters Calculation Time (s)	0.0893	0.2031	0.3634
Total Processing Time (s)	0.1153	0.2291	0.3894

4.6 Discussions

The selection between these two injection types, i.e., impulse injection and PRBS injection, is a trade-off problem. From the system stability point of view, the impulse injection has more negative influence on the system than the PRBS injection. For implementation feasibility, the

impulse injection is easy to implement by one large signal injection or one switching transient in the system, while the PRBS needs the DSP to generate a series of pseudo-random binary sequence signals at each sampling interval. In addition, with impulse injection the estimation results can be obtained right after the transient passes, while with the PRBS injection the estimator requires more transient data to do the iterative calculations, since the injected PRBS signals is usually small. Finally, for better noise tolerance, both impulse and PRBS injections are shown to have good performance in simulation studies, while in practical real-time experiment the PRBS injection shows more stable and reliable performance.

For order selection, it is shown that the RELS processing takes more than 98.0% CPU usage for transfer function of 8th orders and higher, which is not applicable for online estimation in the practical systems. For the considered DSP hardware TMS320F28335, 6th order shows reasonable CPU usage (i.e. 55.8%) as listed in Table 4. 3 and the best noise tolerance as demonstrated in Section 3.3.2.5. Overall, the PRBS injection with transfer function of 6th order is recommended for online implementation of impedance estimation.

Chapter 5: Online Parameters Estimation for Interior Permanent Magnet Synchronous Motors

5.1 Mathematical Modeling of IPMSMs

The next application of the proposed RELS parameter estimation algorithm is the IPMSM driven by the MTPA control, which required accurate knowledge of machine parameters to achieve and maintain its optimal property. Without loss of generality, a three-phase IPMSM is considered with the simplified cross-section diagram shown in Figure 5. 1. It is assumed that the machine has negligible eddy currents and hysteresis losses.

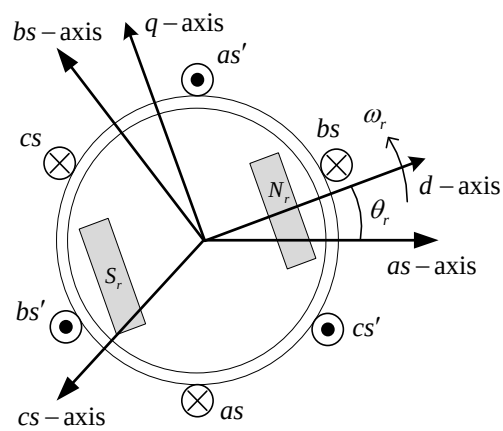

Figure 5. 1 Simplified cross-section diagram of the IPMSM.

The mathematical model of this IPMSM can be described in the synchronous *qd* reference frame, which is shown by the following equations [52]:

$$\begin{cases} v_q = Ri_q + L_q \dfrac{d}{dt} i_q + \omega_e \left(L_d i_d + \lambda_f \right) \\ v_d = Ri_d + L_d \dfrac{d}{dt} i_d - \omega_e L_q i_q \end{cases}, \tag{5.1}$$

where $\mathbf{v}_{q,d}$, $\mathbf{i}_{q,d}$, ω_e are stator voltages, stator currents in *qd* reference frame, and angular velocity of the machine in electrical radiance per second; R, $\mathbf{L}_{q,d}$ and λ_f denote the real stator resistance,

inductances in *qd* frame, and the flux linkage. The electromagnetic torque T_e can be expressed using the stator currents $\mathbf{i}_{q,d}$, flux linkage λ_f, and inductances $\mathbf{L}_{q,d}$ as [52]:

$$T_e = \frac{3}{2} P i_q \left[\left(L_d - L_q \right) i_d + \lambda_f \right] \tag{5.2}$$

where P is the number of pole pairs of the IPMSM.

5.2 MTPA Control Strategy

From (5.2), the electromagnetic torque of the IPMSM is composed of two terms, which are the reluctance torque provided by the magnetic saliency ($L_d \neq L_q$) and the field torque provided by the permanent magnet (PM) flux linkage λ_f. Among these terms, the reluctance torque plays an important role for salient-pole machines. The conventional indirect field-oriented control method with $i_d = 0$ is not best suited for the salient-pole machines, since it will cancel out the reluctance torque term, and cannot minimize the stator current under a given electromagnetic torque.

In IPMSMs, the increase in torque demands may induce larger copper losses, especially for high power machines with high current and torque. Therefore, an efficiency improvement strategy called maximum torque per ampere (MTPA) control is introduced as mentioned in Section 1.1.2, which is able to minimize the total power consumption by making full use of both reluctance torque and PM flux torque.

To study the MTPA operation of an IPMSM, a trajectory of the relationship between i_q and i_d under a given constant torques is illustrated in Figure 5. 2. As seen in Figure 5. 2, the minimum stator current under a given torque constant can be derived by searching for the minimum distance from the origin of the $\mathbf{i}_{q,d}$ coordinate to the torque locus (marked in red).

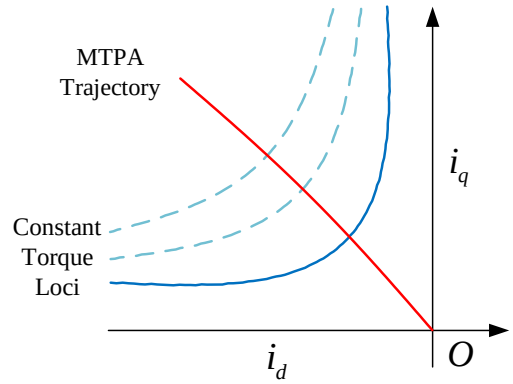

Figure 5. 2 MTPA trajectory for IPMSM.

The diagram of the stator current vector in *qd*-coordinates is demonstrated in Figure 5. 3. The combinations of *q*- and *d*-axes currents under MTPA control can be obtained from the projections of the stator current on *q*- and *d*-axes. The relationship between *q*- and *d*-axes currents and the stator current can be expressed as

$$\begin{cases} i_q = I_s \sin\gamma \\ i_d = I_s \cos\gamma \end{cases}, \tag{5.3}$$

where γ is the current angle.

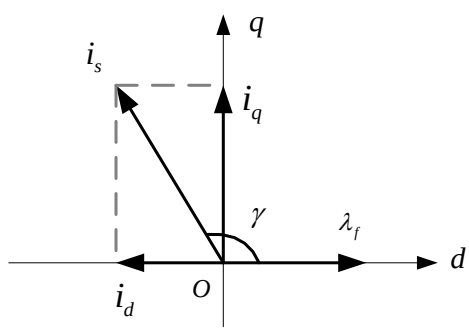

Figure 5. 3 Diagram of the current vector in qd coordinates.

The electromagnetic torque of the machine can be modified by substituting (5.3) into (5.2) as:

$$T_e = \frac{3}{2} P I_s \sin\gamma \left[\left(L_d - L_q \right) I_s \cos\gamma + \lambda_f \right] \tag{5.4}$$

For the MTPA control, the maximum torque produced by a given current angle is calculated by taking the partial derivative of (5.4) with respect to the current angle and setting it to 0 as

$$\frac{\partial T_e}{\partial \gamma} = \frac{3}{2} P I_s \left[\left(L_d - L_q \right) I_s \cos 2\gamma + \lambda_f \cos \gamma \right] = 0 \tag{5.5}$$

Based on (5.3) and (5.5), the following relationship between i_q and i_d under MTPA operation is derived:

$$i_d = \frac{-\lambda_f + \sqrt{\lambda_f^2 + 4\left(L_d - L_q\right)^2 i_q^2}}{2\left(L_d - L_q\right)} \tag{5.6}$$

Substituting (5.3) into (5.6), the optimal current angle γ_M under MTPA operation to achieve the maximum torque as

$$\gamma_M = \arccos \frac{-\lambda_f + \sqrt{\lambda_f^2 + 8\left(L_d - L_q\right)^2 I_s^2}}{4\left(L_d - L_q\right) I_s} . \tag{5.7}$$

5.3 Parameter-Estimation-Based MTPA Control

It is noted that according to (5.7), the optimal angle is depended on machine inductances and PM flux linkage, all of which may vary during motor-drive operation. As noted in Table 2. 1, the second practical application of system identification considered in this thesis is the online parameter estimation for IPMSMs.

5.3.1 RELS Algorithm Design for IPMSM

As seen in (5.1), the mathematical model of the IPMSM contains derivatives of the current $\mathbf{i}_{q,d}$, and hence has to be discretized when applied with the RELS algorithm. Therefore, in terms of Pade approximation method [18], (3) can be discretized as follows:

$$
\begin{cases}
i_q(k) = \theta_{q1} i_q(k-1) + \\
\qquad \theta_{q2}[\omega_e(k) i_d(k) + \omega_e(k-1) i_d(k-1) + \\
\qquad \theta_{q3}[v_q(k) + v_q(k-1)] + \\
\qquad \theta_{q4}[-\omega_e(k) - \omega_e(k-1)] + \\
\qquad e_q(k) \\
i_d(k) = \theta_{d1} i_d(k-1) + \\
\qquad \theta_{d2}[\omega_e(k) i_q(k) + \omega_e(k-1) i_q(k-1) + \\
\qquad \theta_{d3}[v_d(k) + v_d(k-1)] + \\
\qquad e_d(k)
\end{cases}, \tag{5.8}
$$

with the constants $\theta_{q1\text{-}4}$ and $\theta_{d1\text{-}3}$ that appear in (5.8) expressed as

$$
\begin{cases}
\theta_{q1} = \dfrac{-T_s R_s + 2L_q}{T_s R_s + 2L_q} \\
\theta_{q2} = \dfrac{-L_d T_s}{T_s R_s + 2L_q} \\
\theta_{q3} = \dfrac{T_s}{T_s R_s + 2L_q} \\
\theta_{q4} = \dfrac{T_s \lambda_f}{T_s R_s + 2L_q}
\end{cases}, \tag{5.9}
$$

$$
\begin{cases}
\theta_{d1} = \dfrac{-T_s R_s + 2L_d}{T_s R_s + 2L_d} \\
\theta_{d2} = \dfrac{L_q T_s}{T_s R_s + 2L_d} \\
\theta_{d3} = \dfrac{T_s}{T_s R_s + 2L_d}
\end{cases}, \tag{5.10}
$$

where T_s is the sampling period of the discretization. Here, $\mathbf{e}_{q,d}$ are the measurement noise in *qd* reference frame. Based on (5.9), the parameters in the IPMSM can be calculated as,

$$\begin{cases} L_q = \dfrac{(\theta_{q1}+1)T_s}{4\theta_{q3}} \\ L_d = -\dfrac{\theta_{q2}}{\theta_{q3}} \\ \lambda_f = \dfrac{\theta_{q4}}{\theta_{q3}} \end{cases} . \tag{5.11}$$

From the expression of $i_q(k)$ shown in (5.8), the input regression vector and the output equation of the RELS algorithm can be defined as

$$\boldsymbol{\varphi}(k+1) = \begin{bmatrix} i_q(k) \\ \omega_e(k+1)i_d(k+1) + \omega_e(k)i_d(k) \\ v_q(k+1) + v_q(k) \\ -\omega_e(k+1) - \omega_e(k) \\ \varepsilon(k) \end{bmatrix}, \tag{5.12}$$

$$y(k+1) = i_q(k+1), \tag{5.13}$$

with $\boldsymbol{\varphi}$ and y as the regression vector and the output variable, respectively. Since the noise in the system cannot be directly measured, the noise term $e_q(k)$ in (5.8) is replaced by the prediction error $\varepsilon(k)$. Based on (5.8), (5.9), (5.12), and (5.13), the estimated output variable can be expressed using the following equation:

$$\hat{y}(k+1) = \boldsymbol{\varphi}^T(k+1)\hat{\boldsymbol{\theta}}(k). \tag{5.14}$$

And $\hat{\boldsymbol{\theta}}$ is the estimated parameter vector with the components shown as follows:

$$\hat{\boldsymbol{\theta}}^T(k) = \begin{bmatrix} \theta_{q1} & \theta_{q2} & \theta_{q3} & \theta_{q4} & c_1 \end{bmatrix}. \tag{5.15}$$

The input $\boldsymbol{\varphi}$ (k+1) and output y(k+1) signals are fed into the RELS algorithm which has been introduced in Section 2.1.2.2.

The block diagram of the parameter vector estimation is illustrated in Figure 5. 4, where the RELS algorithm allows the estimated parameters of the system to be updated at each sampling

interval as the new data become available. The estimated output $\hat{y}$ (k+1) obtained by RELS algorithm is compared with the measured output y(k+1) to generate a prediction error ε(k+1) that in turn updates the parameters of the model. Such parameter updating mechanism is known as recursive "predictor-corrector" calculation that greatly decreases the computational complexity of the algorithm. By recursively calculating the parameters $\boldsymbol{\theta}_{q1\text{-}4}$ in (5.9), the q- and d-axes inductances $L_{q,d}$ and the flux linkage λ_f of the machine can be online updated using (5.11).

Since the RELS is sensitive the accuracy of the measured signal, any harmonics, ripple, and noise will influence the accuracy of the estimated results. A commonly used low pass-filter is not be recommended here, because the overshoot in the high frequency would be filtered, which will significantly influence the accuracy of estimation. Therefore, a moving average algorithm with sliding time window for 10 samples is applied here to reduce the negative influence of unwanted data.

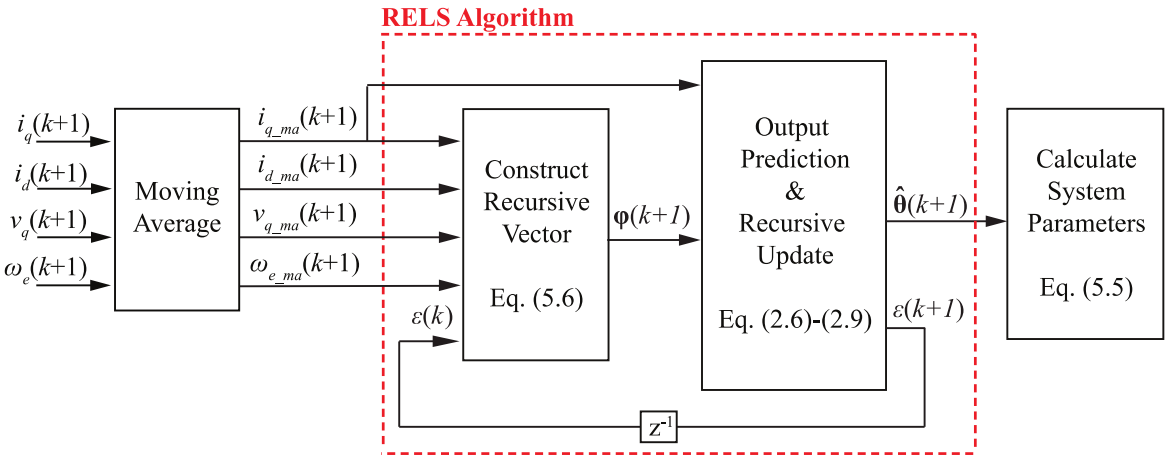

Figure 5. 4 Block diagram of the parameter estimation based on RELS algorithm.

5.3.2 Modifications of Basic RELS Algorithm for Tracking Parameters Variation

5.3.2.1 Random Walk

Since there is no excitation when the IPMSM is operating in steady-state, the covariance matrix will become relatively small and the new parameters cannot be identified properly. A symmetric positive definite matrix **R** can be added to the covariance matrix **P** for one iteration once a large prediction error is detected (i.e. $\varepsilon(k+1)>0.6$) as [19]:

$$\mathbf{R} = r_0 \mathbf{I}_m , \tag{5.16}$$

where r_0 is the random walk constant, m is the dimensions of matrix **P**, and $\mathbf{I}_m$ is a mth order identity matrix. In this thesis, the trace value of **P** is approximately 10^{-4}. Since the variation range of the machine parameters is usually within ±100%, r_0 is selected as 10^{-4} for stability consideration.

5.3.2.2 Modified Forgetting Factor

Forgetting factor λ the most commonly used technique to decrease the influence of old samples through providing them with less weight [19]. The function of the forgetting factor applied here is to improve the convergence speed when the parameters are varying. Incorporating the forgetting factor into the RELS, the gain and covariance matrix can be modified as

$$\mathbf{K} = \frac{\mathbf{P}(k)\boldsymbol{\varphi}(k+1)}{\lambda + \boldsymbol{\varphi}^T(k+1)\mathbf{P}(k)\boldsymbol{\varphi}(k+1)} , \tag{5.17}$$

$$\mathbf{P}(k+1) = \mathbf{P}(k)\left[\mathbf{I} - \boldsymbol{\varphi}(k+1)\mathbf{K}^T\right]/\lambda . \tag{5.18}$$

The value of λ is recommended to be selected between 0.95 and 0.9999 after the RELS algorithm switches into stable operation mode. Lower values may be suitable to accelerate the convergence speed, while dropping λ too much may lead to the covariance matrix growing rapidly and the estimator results blowing up. In practical cases, such forgetting factor technique requires

consecutive excitations into the estimated system to avoid estimator wind-up, which is not feasible for steady-state operation of the IPMSM. Therefore, a modification of the forgetting factor is presented here only for the situations when a large prediction error is detected (i.e. $\varepsilon(k+1)>0.6$) [20]:

$$\lambda(t) = \lambda_0 + (1-\lambda_0)\left[1-\exp(\frac{-t}{\tau})\right], \tag{5.19}$$

where λ_0 is the initial forgetting factor, τ is the time constant for determining the time for the forgetting factor to reach 1.

5.3.3 Speed Servo Control System Design

The block diagram of the considered speed servo motor drive system incorporating online parameter estimation strategy is demonstrated in Figure 5. 5. Therein, the online parameter estimator is adopted to estimate the *q*- and *d*-axes inductances $\mathbf{L}_{q,d}$ and the flux linkage λ_f at each sample interval through RELS algorithm as introduced in Section 5.2. The values of $\mathbf{L}_{q,d}$ and λ_f are the estimated parameters based on (5.3) and (5.7). The speed control applied here is the indirect field-oriented control (IFOC) [52]. This control is implemented through decoupling the torque component and flux component provided by IPMSM through *qd* axes. Then, the ac motor is controlled as a dc motor through double closed-loop control. The outer loop is a PI controller for speed reference tracking, while the inner loop is two PI controllers for current (i.e. $\mathbf{i}_{q,d}$) regulation. The outputs of the IFOC control are the voltage signals that are fed into the space vector pulse-width modulation (SVPWM) to provide appropriate switching signals for the insulated gate bipolar transistors (IGBTs) in the inverter. High accuracy MTPA control of the IPMSM under parameter

variations can be guaranteed using the proposed parameter-estimation-based adaptive MTPA control strategy.

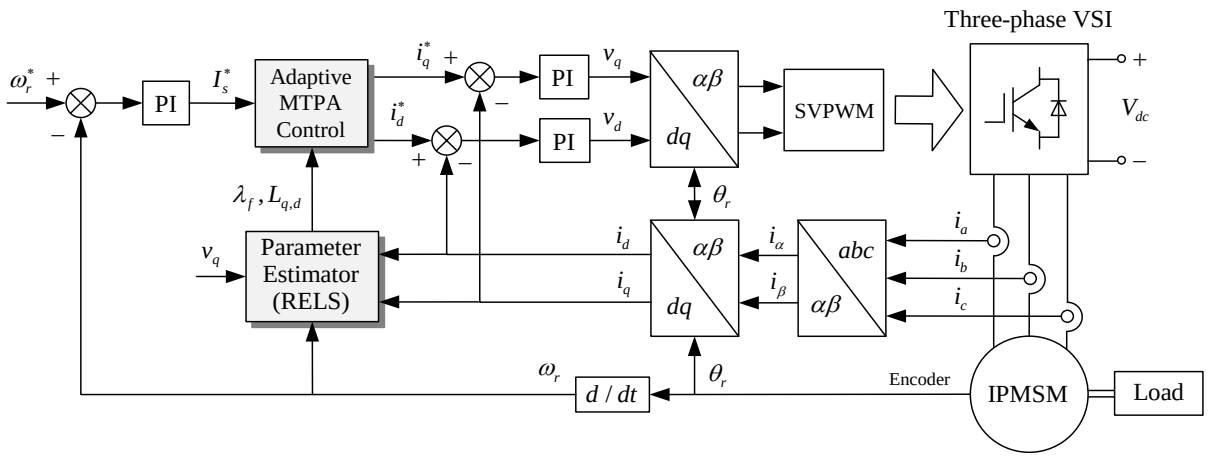

Figure 5. 5 Block diagram of the speed servo motor drive control system with parameter-estimation-based adaptive MTPA control strategy.

Chapter 6: Performance of Parameter-Estimation-Based Adaptive MTPA Control

6.1 System Description

To demonstrate the effectiveness of the proposed parameter-estimation-based adaptive MTPA control strategy, a 300kW IPMSM with the speed servo control system (as illustrated in Figure 5. 5) is modeled using MATLAB/Simulink. The parameters of the IPMSM and PI controllers are listed in Appendix D.

6.2 Initialization of Parameter Estimator

The sampling frequency of the moving average block is set to 100 kHz, and the sampling frequency of RELS algorithm is set as 10 kHz. Since some estimated parameters are relatively small, the initial setting for the parameter vector $\boldsymbol{\theta}(0)$ is set as a zero vector, and the covariance $\mathbf{P}(0) = 10^{-4}\mathbf{I}_5$. After the estimator reaches the convergence, the prediction error of will be around ±0.1. Then, the estimated machine parameters can be used for the adaptive MTPA controller design until the next convergence.

Once the parameters of identified system changes, the algorithm will calculate a large predicted error (i.e. $\varepsilon(k+1) > 0.6$). Then the algorithm will apply random walk technique and modified forgetting factor to track the parameters variation. Since the trace of the covariance matrix P is around 10^{-4} during the steady state operation of the IPMSM, the values of random walk $\mathbf{R}$ are selected as follows to avoid large transients during the estimation,

$$\mathbf{R} = 10^{-4}\mathbf{I}_5 . \tag{6.1}$$

The modified forgetting factor $\lambda(t)$ is set as,

$$\lambda(t) = 0.9994 + 0.0006(1 - e^{-t/0.5}) . \tag{6.2}$$

Once the prediction error keeps within ±0.2, the new estimated parameters will be updated in the adaptive MTPA controller.

6.3 Case 1: Performance under Machine Change

The reference mechanical speed of the IPMSM and the load torque are set to 800r/min and 500Nm. At the start, the machine parameters are assumed to correspond to a given motor (labeled as the old motor). The old motor is assumed to operate with the proposed adaptive MTPA control strategy under steady state at 800r/min. The online parameters estimator through the RELS algorithm has been employed to estimate the *q*- and *d*-axes inductances and the flux linkage and reached the convergence. To examine the tracking capability of the proposed estimator, the operating IPMSM is assumed to be replaced (e.g. due to failure) at t = 0s by a new machine that has a slightly different parameter. The new *q*- and *d*-axes inductances L_{q2}, L_{d2}, and the new flux linkage λ_{f2} are listed in Appendix D. The purpose of this study is to investigate the performance of the parameter estimation algorithm under a sudden change of several parameters. The performance of the parameter-estimation-based adaptive MTPA control of this case study are shown in Figure 6. 1.

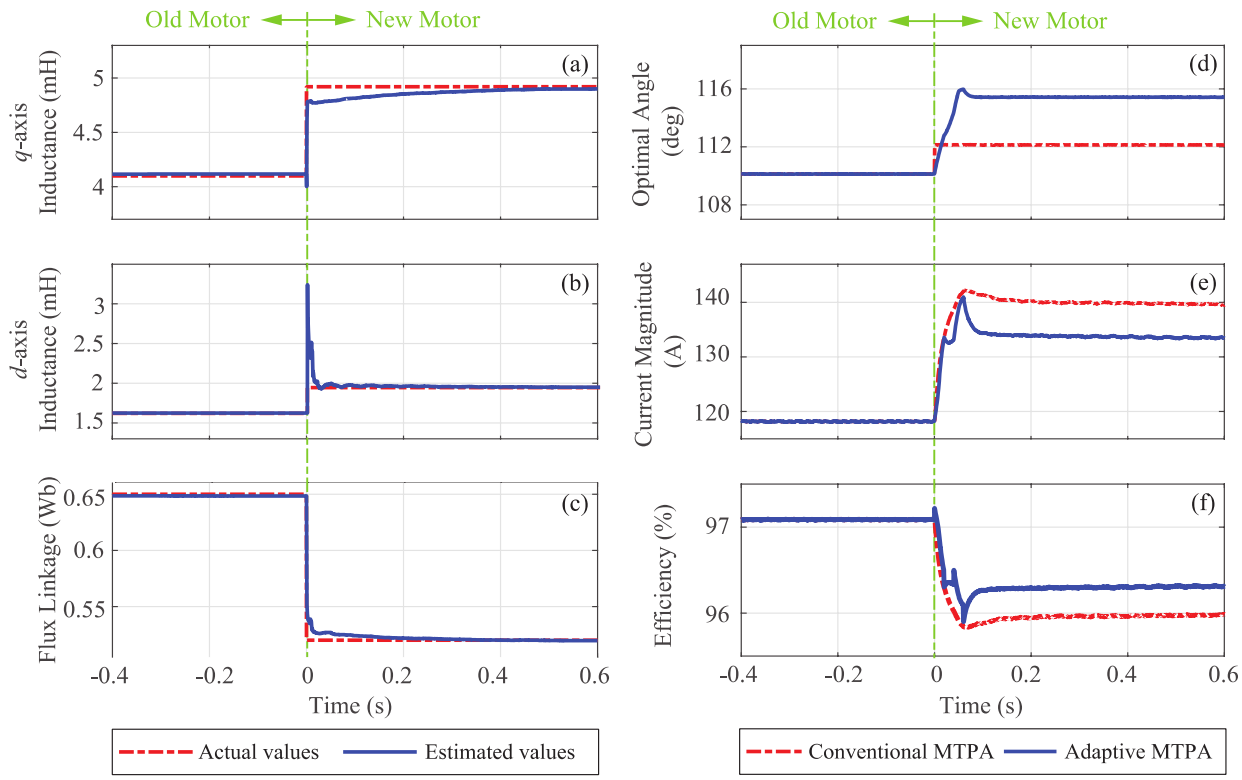

Figure 6. 1 Simulation results under motor changes: (a) L_q, (b) L_d, and (c) λ_f , (d) optimal current angle, (e) magnitude of the stator current, (f) efficiency of the motor.

As shown in Figure 6. 1 (a-c), for the old machine, the inductances and flux linkage are estimated as 4.0mH, 1.6mH, and 0.648Wb, which have the relative error of 2.4%, 1.2%, and 0.3%, respectively. After the machine is being replaced by a different one, the estimator takes 0.2s to converge, and the new parameters are estimated as 5.0mH, 1.9mH, and 0.519Wb, with the relative error of 1.6%, 2.3%, and 0.2%, respectively. As shown in Figure 6. 1(a), for the new machine parameters, the optimal current angle is updated to 115.5° using the proposed MTPA control, while the result from conventional MTPA method is 112.1°. This 3.4° increment helps the system to reduce the current magnitude from 140.1A to 133.4A (as shown in Figure 6. 1(e)) and improve the efficiency from 95.9% to 96.3% (as shown in Figure 6. 1(f)). In contrast, the conventional MTPA

has compromised optimal control performance with less accurate MTPA operation and lower efficiency.

6.4 Case 2: Performance under Load Torque Change

To further assess the robustness of the proposed control strategy, a transient study composed of several load changes is assumed here. First, the new motor is assumed to operate in a steady state loaded with 400Nm. At t = 0.2s, the load torque of the new IPMSM is changed from 400Nm to 800Nm; then, at t = 0.7s, to 600Nm; and finally, at t = 1.2s, the load torque is changed back to 400Nm. The estimated parameters and the results for the adaptive MTPA control of this case study are illustrated in Figure 6. 2. As observed in Figure 6. 2(a)-(c), the relative estimation error of each parameter are approximately 0.8%, 0.5%, and 0.4%, with slight fluctuations during the torque changes. The adaptive MTPA algorithm updates the optimal current angle to 114.6°, 120.9° and 118.6° (as shown in Figure 6. 2(d)) under the load torques of 400Nm, 800Nm, and 600Nm, and minimizes the current magnitude to 111.4A, 190.8A and 154.2A (as shown in Figure 6. 2(e)), which ensures a high-efficiency operation of the machine under different loads. These results imply that the accuracy of the parameter identification is not affected by the load torque, and the robustness of the proposed algorithm is verified.

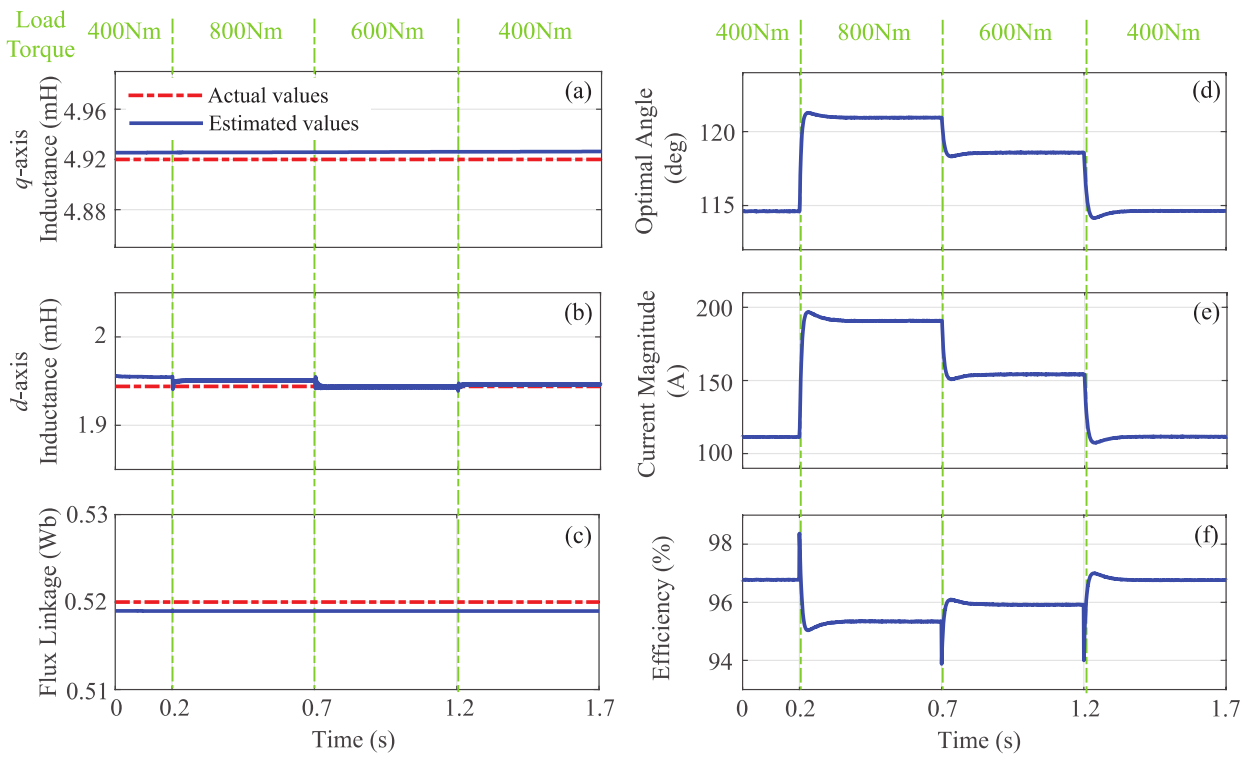

Figure 6. 2 Simulation results under load torque changes: (a) L_q, (b) L_d, and (c) λ_f , (d) optimal current angle, (e) magnitude of the stator current, (f) efficiency of the motor.

Chapter 7: Conclusions and Future Work

7.1 Conclusions and Contributions

The stability issues in dc distribution systems caused by power electronic loads will become increasingly important in the future because of the proliferation of dc technology and related applications. To design the adaptive stabilizers for the interconnection interfaces, the detailed information of impedances of sources and loads is required. To address this issue, a new method for online estimation of the source impedance in dc distribution systems has been proposed here. **Objective 1,** as addressed in Chapter 2 and Chapter 3, proposes a new online impedance identification method based on the RELS analysis of the system transient response, after applying an impulse or PRBS injections. This kind of online impedance estimation based on RELS algorithm incorporating transfer function reconstruction, can be specifically designed for SISO systems, and is able to significantly reduce the sensitivity to the noise. Compared with the established DFT method, the proposed RELS method features benefits of the direct parametric solution, better resilience to noise in the high frequency range, and lower requirement on stored data and processing time. The detailed performance comparison between impulse injection and PRBS injection includes accuracy in numerical performance, parameters estimation and noise tolerance have been presented to support the proposed methodology.

In Chapter 4, **Objective 2** was achieved by implementation of the proposed RELS method in the HIL platform. The performance of the programmed parameter estimator in DSP including CPU usage with different order selection, and time cost have been presented and analyzed. The recommended configuration for online impedance estimation implementation is concluded. Therefore, the proposed online parameter estimator is validated as a feasible and robust tool that

can be considered for future implementation in adaptive controllers of sources and loads in dc distribution systems.

The **Objective 3** aims to mitigate the impact of parameter variations on the MTPA operation of the IPMSM motor drive systems. For achieving this goal using the proposed RELS method, the parameter-estimation-based adaptive MTPA control strategy has been proposed in Chapter 5 and Chapter 6. This method is designed to online estimate the *q*- and *d*-axes inductances and the permanent magnet flux linkage that are required in the calculation of the optimal current angle in MTPA control. The random walk and modified forgetting factor techniques are incorporated with the RELS algorithm to improve the tracking accuracy during the parameter variations. Simulation results verify that the proposed algorithm estimates the inductances and flux linkage of the IPMSM with reasonable accuracy, while achieving a high-efficiency MTPA operation of the machine under large variations of several key parameters.

7.2 Future Work

To conclude this thesis, there are several areas for potential extension of the proposed work:

- **Design online parameter-estimation-based adaptive stabilizers for dc distribution systems**

  The proposed online source impedance estimator based on RELS is verified as a robust and feasible tool to estimate the parameters of the sources. Therefore, this method can be used for design of adaptive stabilizers and online tuning of sources and loads controllers, which is one of the motivations as discussed in Section 1.1.1. Based on the estimated parameters and known impedance of the load side, an adaptive damper can be designed to reshape the impedance of

the source/load side through current injection/absorbing to make the interconnection meet the impedance-based stability criteria.

- **Experiment validation for parameter-estimation-based adaptive MTPA control for interior permanent magnet synchronous motors**

  The effectiveness and robustness of the proposed adaptive MTPA control method have been examined by computer studies. However, since the sensitivity of RELS algorithm, the feasibility of this parameter estimator needs to be further validated in experimental (hardware) environment. Moreover, the proposed RELS algorithm can also be applied for online parameter estimation of sensor-less induction motor drives.

Future researches on these or other topics are currently considered by other graduate students of the UBC's Electrical Power and Energy Systems research group.

References

[1] A. M. Rahimi and A. Emadi, "An analytical investigation of dc/dc power electronic converters with constant power loads in vehicular power systems," *IEEE Trans. Veh. Technol.*, vol. 58, no. 6, pp. 2689-2702, Jul. 2009.

[2] A. Alacano, J. J. Valera, G. Abad and P. Izurza, "Power-electronic-based dc distribution systems for electrically propelled vessels: a multivariable modeling approach for design and analysis," *IEEE Trans. Emerg. Sel. Topics Power Electron.*, vol. 5, no. 4, pp. 1604-1620, Dec. 2017.

[3] R. Quigley, " More electric aircraft," in *Proc. IEEE Applied Power Electron. Conf. (APEC)*, 1993, pp. 906-911.

[4] G. Byeon, T. Yoon, S. Oh and G. Jang, "Energy management strategy of the dc distribution system in buildings using the EV service model," *IEEE Trans. Power Electron.*, vol. 28, no. 4, pp. 1544-1554, April 2013.

[5] A. Emadi and M. Ehsani, "Multi-converter power electronic systems: definition and applications," *2001 IEEE 32nd Annual Power Electron. Spec. Conf. (PESC)*, Vancouver, BC, 2001, vol. 2, pp. 1230-1236.

[6] J. Sun, "Impedance-based stability criterion for grid-connected inverters," in *IEEE Trans. Power Electron.*, vol. 26, no. 11, pp. 3075-3078, Nov. 2011.

[7] M. B. Harris, A. W. Kelley, J. P. Rhode and M. E. Baran, "Instrumentation for measurement of line impedance," *1994 Applied Power Electron. Conf. and Expo. (APEC)*, Orlando, FL, 1994, vol.2., pp. 887-893.

[8] M. Khayamy and H. Chaoui, "Efficient PMSM inverter-based frive for vehicular transportation systems," *IEEE Trans. Veh. Technol.*, vol. 67, no. 6, pp. 4783-4792, Jun. 2018.

[9] C. Calleja, A. Lopez-de-Heredia, H. Gaztanaga, L. Aldasoro, and T. Nieva, "Validation of a modified direct self control strategy for PMSM in railway-traction applications," *IEEE Trans. Ind. Electron.*, vol. 63, no. 8, pp. 5143-5155, Aug. 2016.

[10] Q. Liu and K. Hameyer, "High-performance adaptive torque control for an IPMSM with real-time MTPA operation," *IEEE Trans. Energy Convers.*, vol. 32, no. 2, pp. 571-581, Jun. 2017.

[11] R. Pintelon and J. Schoukens, *System Identification- A Frequency Domain Approach*. New York, NY, USA: IEEE, 2001.

[12] P. E. Wellstead and M. B. Zarrop. *Self-tuning Systems: Control and Signal Processing.* John Wiley & Sons, 1991.

[13] K. J. Aström and B. Wittenmark, Adaptive Control Second Edition. Boston, MA: Addison-Wesley, 1995.

[14] D. I. Wilson, *Advanced Control using Matlab: Or Stabilising the Unstabilisable*, Auckland University of Technology, 2016.

[15] Z. Staroszczyk, "A method for real-time, wide-band identification of the source impedance in power systems," *IEEE Trans. Instrum. Meas.*, vol. 54, no. 1, pp. 377-385, Feb. 2005.

[16] M. Céspedes and J. Sun, "Online grid impedance identification for adaptive control of grid-connected inverters," *2012 IEEE Energy Convers. Cong. Expo. (ECCE)*, Raleigh, NC, 2012, pp. 914-921.

[17] J. Siegers and E. Santi, "Stability analysis and control design for an all-electric ship MVDC power distribution system using a passivity based stability criterion and power hardware-in-the-loop simulation," *2015 IEEE Electr. Ship Technol. Sym. (ESTS)*, Alexandria, VA, 2015, pp. 86-92.

[18] D. Serfontein, J. Rens, G. Botha and J. Desmet, "Continuous event-based harmonic impedance assessment using online measurements," in *IEEE Trans. Instrum. Meas.*, vol. 65, no. 10, pp. 2214-2220, Oct. 2016.

[19] A. Riccobono, E. Liegmann, M. Pau, F. Ponci and A. Monti, "Online parametric identification of power impedances to improve stability and accuracy of power hardware-in-the-loop simulations," in *IEEE Trans. Instrum. Meas.*, vol. 66, no. 9, pp. 2247-2257, Sept. 2017.

[20] M. Sumner, B. Palethorpe, D. W. P. Thomas, P. Zanchetta and M. C. Di Piazza, "A technique for power supply harmonic impedance estimation using a controlled voltage disturbance," in *IEEE Trans. Power Electron.*, vol. 17, no. 2, pp. 207-215, March 2002.

[21] M. Jordan, H. Langkowski, T. D. Thanh and D. Schulz, "Frequency dependent grid-impedance determination with pulse-width-modulation-signals," *2011 7th Intl. Conf. Workshop Comp. Power Electron. (CPE)*, Tallinn, 2011, pp. 131-136.

[22] D. Martin, E. Santi and A. Barkley, "Wide bandwidth system identification of ac system impedances by applying pertubations to an existing converter," *2011 IEEE Energy Convers. Cong. Expo. (ECCE)*, Phoenix, AZ, 2011, pp. 2549-2556.

[23] A. Riccobono *et al*., "Stability of shipboard dc power distribution: online impedance-based systems methods," in *IEEE Electrification Mag.*, vol. 5, no. 3, pp. 55-67, Sept. 2017.

[24] T. Roinila, M. Vilkko and J. Sun, "Broadband methods for online grid impedance measurement," *2013 IEEE Energy Convers. Cong. Expo. (ECCE)*, Denver, CO, 2013, pp. 3003-3010.

[25] T. Roinila, M. Vilkko and J. Sun, "Online Grid Impedance Measurement Using Discrete-Interval Binary Sequence Injection," *IEEE Trans. Emerg. Sel. Topics Power Electron.*, vol. 2, no. 4, pp. 985-993, Dec. 2014.

[26] T. Roinila and T. Messo, "Online grid-impedance measurement using ternary-sequence injection," in *IEEE Trans. Ind. Appl.*, vol. 54, no. 5, pp. 5097-5103, Sept.-Oct. 2018.

[27] T. Roinila *et al*., "Hardware-in-the-loop methods for real-time frequency-response measurements of on-board power distribution systems," in *IEEE Trans. Ind. Electron.*, to appear.

[28] T. Roinila, H. Abdollahi, S. Arrua and E. Santi, "Real-time stability analysis and control of multi-converter systems by using MIMO-identification techniques," in *IEEE Trans. Power Electron.*, to appear.

[29] T. Roinila, T. Messo and E. Santi, "MIMO-identification techniques for rapid impedance-based stability assessment of three-phase systems in DQ domain," in *IEEE Trans. Power Electron.*, vol. 33, no. 5, pp. 4015-4022, May 2018.

[30] R. Luhtala, T. Roinila and T. Messo, "Implementation of real-time impedance-based stability assessment of grid-connected systems using MIMO-identification techniques," in *IEEE Trans. Ind. Appl.*, vol. 54, no. 5, pp. 5054-5063, Sept.-Oct. 2018.

[31] J. Yang, W. Li, T. Chen, W. Xu and M. Wu, "Online estimation and application of power grid impedance matrices based on synchronised phasor measurements," in *IET Gen. Transmission & Distrib.*, vol. 4, no. 9, pp. 1052-1059, September 2010.

[32] J. Xia, N. Amiri, and J. Jatskevich, "An adaptive MTPA control method for interior permanent magnet synchronous motors considering demagnetization and temperature effects," *2018 9th IEEE Annual Inf. Technol., Electron. Mobile Commun. Conf. (IEMCON)*, Vancouver, BC, 2018.

[33] K. Li and Y. Wang, "Maximum torque per ampere (MTPA) control for IPMSM drives based on a variable-equivalent-parameter MTPA control law," in *IEEE Trans. Power Electron.*, to appear.

[34] C. Lai, G. Feng, K. Mukherjee, V. Loukanov, and N. C. Kar, “Torque ripple minimization for interior PMSM with consideration of magnetic saturation incorporating online parameter identification,” *IEEE Trans. Magn.*, vol. 53, no. 6, pp. 1-4, Jun. 2017.

[35] Hyunbae Kim, J. Hartwig and R. D. Lorenz, "Using on-line parameter estimation to improve efficiency of IPM machine drives," *2002 IEEE 33rd Annual IEEE Power Electron. Spec. Conf.. (PESC)*, Cairns, Qld., Australia, 2002, pp. 815-820 vol.2.

[36] P. Niazi, H. A. Toliyat and A. Goodarzi, "Robust maximum torque per ampere (MTPA) control of PM-assisted SynRM for traction applications," in *IEEE Trans. Veh. Technol.*, vol. 56, no. 4, pp. 1538-1545, July 2007.

[37] Y. A. -. I. Mohamed and T. K. Lee, "Adaptive self-tuning MTPA vector controller for IPMSM drive system," in *IEEE Trans. Energy Convers.*, vol. 21, no. 3, pp. 636-644, Sept. 2006.

[38] M. S. Rafaq, F. Mwasilu, J. Kim, H. H. Choi and J. Jung, "Online parameter identification for model-based sensorless control of interior permanent magnet synchronous machine," in *IEEE Trans. Power Electron.*, vol. 32, no. 6, pp. 4631-4643, June 2017.

[39] K. Makara, R. Jérémi, and F. Jean, “Detection of turn short-circuit faults in stator of PMSM by on-line parameter estimation,” in *Proc. Int. Symp. Power Electron., Elect. Drives, Autom. Motion*, Jun. 2008, pp. 161-166.

[40] S. Kim *et al*., "Torque ripple improvement for interior permanent magnet synchronous motor considering parameters with magnetic saturation," in *IEEE Trans.Magn.*, vol. 45, no. 10, pp. 4720-4723, Oct. 2009.

[41] S. J. Underwood and I. Husain, "Online parameter estimation and adaptive control of permanent-magnet synchronous machines," in *IEEE Trans. Ind. Electron.*, vol. 57, no. 7, pp. 2435-2443, July 2010.

[42] Q. Liu and K. Hameyer, "High-performance adaptive torque control for an IPMSM with real-time MTPA operation," in *IEEE Trans. Energy Convers.*, vol. 32, no. 2, pp. 571-581, June 2017.

[43] Z. Liu, H. Wei, X. Li, K. Liu and Q. Zhong, "Global identification of electrical and mechanical parameters in PMSM drive based on dynamic self-learning PSO," in *IEEE Trans. Power Electron.*, vol. 33, no. 12, pp. 10858-10871, Dec. 2018.

[44] HARDWARE-IN-THE-LOOP, OPAL-RT Technologies, Inc., Montreal, Quebec, Canada, 2018. [Online]. Available: http://www.opal-rt.com/hardware-in-the-loop. (Consulted on Jan. 08, 2019).

[45] RT-LAB (v11.3.1.34), OPAL-RT Technologies, Inc., Montreal, Quebec, Canada

[46] MATLAB (R2018b), The MathWorks, Inc., Natick, MA, USA, 2018.

[47] Simulink –User's Manual, The MathWorks, Inc., Natick, MA, USA, 2018.

[48] LabView 2017, National Instruments, Austin, Texas, USA, 2017.

[49] P. Fraigniaud, "The Durand-Kerner polynomials roots-finding method in case of multiple roots," in *BIT Numerical Mathematics*, vol. 31, no. 1, pp. 112-123, Mar. 1991.

[50] J. Zhang, J. S. Lai, R. Y. Kim and W. Yu, "High-power density design of a soft-switching high-power bidirectional dc-dc converter," *IEEE Trans. Power Electron.*, vol. 22, no. 4, pp. 1145-1153, July 2007.

[51] O. Pizniur, Z. Shan and J. Jatskevich, "Flyback-converter-based source identification for investigation of dynamic stability with constant power loads," *2015 IEEE 16th Workshop on Control and Modeling Power Electron. (COMPEL)*, Vancouver, BC, 2015, pp. 1-7

[52] P. C. Krause, O. Wasynczuk, and S. D. Pekarek, Electromechanical Motion Devices. Piscataway, NJ, USA: Wiley-IEEE Press, 2012.

Appendices

Appendix A Parameters of the Source System in Scenario A and Scenario B

Flyback DC/DC Converter	
Input voltage range (v_g)	42-60 VDC
Output voltage range (v_o)	24-27 VDC
Switching frequency	130 kHz
Output impedance (R_o)	0.014 Ω
Transmission Cable	
Parasitic resistance (R_{tl})	0.082 Ω
Parasitic inductance (L_{tl})	92 μH
Damping Circuit	
Passive damping resistance (R_d)	0.12 Ω
Passive damping capacitance (C_d)	1000 μF

Appendix B Parameters of the Passive Load System in Scenario A

Parameters	Values
Perturbation resistance (R_{petb})	4 Ω
Switch resistance (R_{sw})	0.37 Ω

Appendix C Parameters of the Active Load System in Scenario B

Parameters	Values
Type	Synchronous buck
Input voltage range	20-30 V
Output voltage range	5-30 V
Switching frequency	10 kHz
Controller type	Duty cycle voltage regulated
Main inductor (L_{bm})	100 μH
Main capacitor (C_{bm})	1 mF
Coefficients for voltage PI controller (k_p, k_i)	0.2, 20
Inductance of input filter (L_{fi})	120 μH
Capacitance of input filter (C_{fi})	3 mF

Appendix D Parameters for Controllers and IPMSM

Parameters	Values
Maximum power	300kW
Rated current	300A
DC-link voltage	1500V
Pole pairs (P)	4
Stator resistance of old motor (R_{s1})	0.0459Ω
d-axis inductance of old motor (L_{d1})	1.62mH
q-axis inductance of old motor (L_{q1})	4.1mH
Flux linkage of old motor (λ_{f1})	0.65Wb
Stator resistance of new motor (R_{s2})	0.05508Ω
d-axis inductance of new motor (L_{d2})	1.94mH
q-axis inductance of new motor (L_{q2})	4.92mH
Flux linkage of new motor (λ_{f2})	0.52Wb
Coefficients for speed PI controller (k_{p1}, k_{i1})	15, 50
Coefficients for current PI controllers ($k_{p2,3}$, $k_{i2,3}$)	30, 50